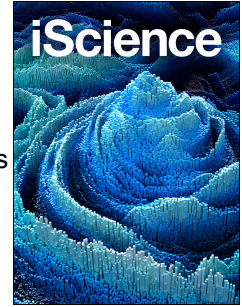




Since January 2020 Elsevier has created a COVID-19 resource centre with free information in English and Mandarin on the novel coronavirus COVID-19. The COVID-19 resource centre is hosted on Elsevier Connect, the company's public news and information website.

Elsevier hereby grants permission to make all its COVID-19-related research that is available on the COVID-19 resource centre - including this research content - immediately available in PubMed Central and other publicly funded repositories, such as the WHO COVID database with rights for unrestricted research re-use and analyses in any form or by any means with acknowledgement of the original source. These permissions are granted for free by Elsevier for as long as the COVID-19 resource centre remains active.

# Journal Pre-proof



Versatile live-attenuated SARS-CoV-2 vaccine platform applicable to variants induces protective immunity

Akiho Yoshida, Shinya Okamura, Shiho Torii, Sayuri Komatsu, Paola Miyazato, Hitomi Sasaki, Shiori Ueno, Hidehiko Suzuki, Wataru Kamitani, Chikako Ono, Yoshiharu Matsuura, Shiro Takekawa, Koichi Yamanishi, Hiroataka Ebina

PII: S2589-0042(22)01684-4

DOI: <https://doi.org/10.1016/j.isci.2022.105412>

Reference: ISCI 105412

To appear in: *ISCIENCE*

Received Date: 7 July 2022

Revised Date: 13 September 2022

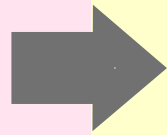
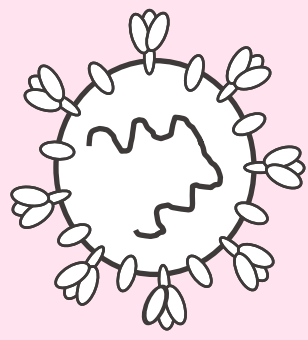
Accepted Date: 18 October 2022

Please cite this article as: Yoshida, A., Okamura, S., Torii, S., Komatsu, S., Miyazato, P., Sasaki, H., Ueno, S., Suzuki, H., Kamitani, W., Ono, C., Matsuura, Y., Takekawa, S., Yamanishi, K., Ebina, H., Versatile live-attenuated SARS-CoV-2 vaccine platform applicable to variants induces protective immunity, *ISCIENCE* (2022), doi: <https://doi.org/10.1016/j.isci.2022.105412>.

This is a PDF file of an article that has undergone enhancements after acceptance, such as the addition of a cover page and metadata, and formatting for readability, but it is not yet the definitive version of record. This version will undergo additional copyediting, typesetting and review before it is published in its final form, but we are providing this version to give early visibility of the article. Please note that, during the production process, errors may be discovered which could affect the content, and all legal disclaimers that apply to the journal pertain.

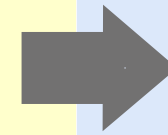
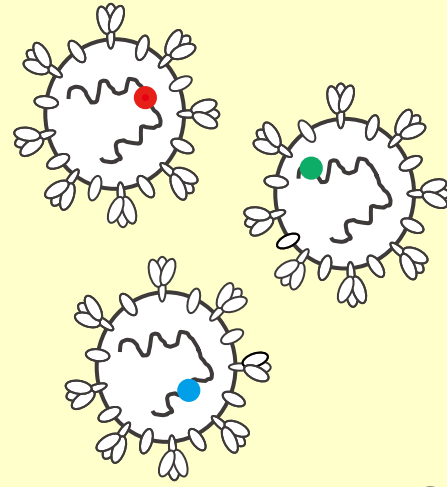
© 2022

Wild type  
virus



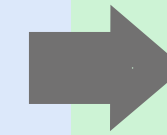
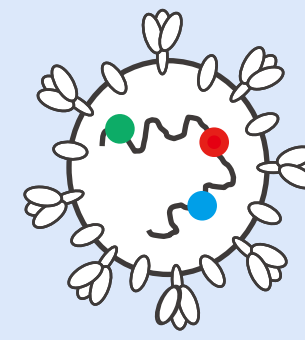
Mutagenesis

Temperature-sensitive  
mutants



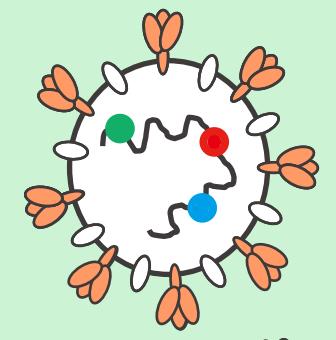
CPER  
recombination

Engineered  
temperature-sensitive  
virus



Spike exchange  
in 2 weeks

Versatile live-attenuated  
vaccine platform



Spike  
CoV-X

Proliferation at 37°C

+++

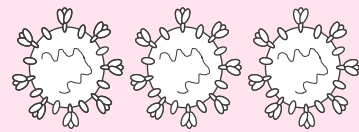
+ / -

-

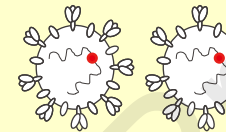
-

Viral load

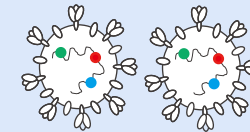
Nasal cavity



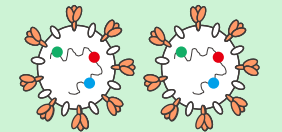
+++



++

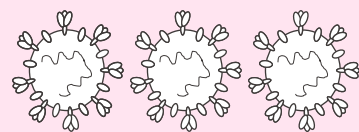


++

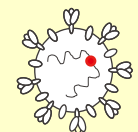


++

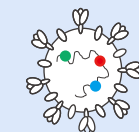
Lungs



+++



+



+



+

Risk of  
virulence reversion

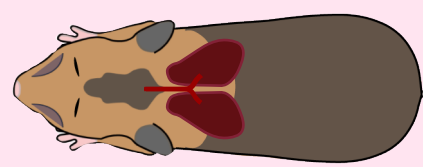
Not applicable

High

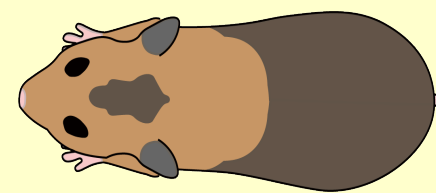
Low

Low

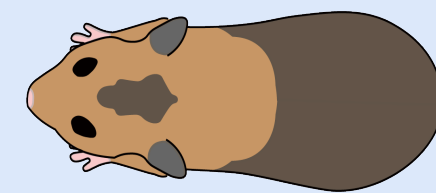
Pathogenicity



Tissue damage  
Weight decrease



No weight decrease



No weight decrease



No weight decrease

Nasal wash  
nAb titer

+++

Not determined

+++

Not determined

Titer

+++

+++

+++

+++

Serum  
nAbs

Persistence

Not determined

Maintained for up to 4 months

Not determined

Not determined



1 **Versatile live-attenuated SARS-CoV-2 vaccine platform applicable to variants**  
2 **induces protective immunity**

3  
4 Akiho Yoshida<sup>1, 2, 7</sup>, Shinya Okamura<sup>1, 2, 7</sup>, Shiho Torii<sup>3, 4</sup>, Sayuri Komatsu<sup>1, 2</sup>, Paola Miyazato<sup>1, 2</sup>,  
5 Hitomi Sasaki<sup>2</sup>, Shiori Ueno<sup>5</sup>, Hidehiko Suzuki<sup>1, 2</sup>, Wataru Kamitani<sup>5</sup>, Chikako Ono<sup>3, 4</sup>, Yoshiharu  
6 Matsuura<sup>3, 4</sup>, Shiro Takekawa<sup>2</sup>, Koichi Yamanishi<sup>2</sup> and Hirotaka Ebina<sup>1, 2, 6, 8\*</sup>

7  
8 <sup>1</sup>Virus Vaccine Group, BIKEN Innovative Vaccine Research Alliance Laboratories, Institute for Open  
9 and Transdisciplinary Research Initiatives, Osaka University, Suita, Osaka, Japan

10 <sup>2</sup>The Research Foundation for Microbial Diseases of Osaka University, Suita, Osaka, Japan

11 <sup>3</sup>Laboratory of Virus Control, Research Institute for Microbial Diseases, Osaka University, Suita,  
12 Osaka, Japan

13 <sup>4</sup>Laboratory of Virus Control, Center for Infectious Disease Education and Research, Osaka University,  
14 Suita, Osaka, Japan

15 <sup>5</sup>Department of Infectious Diseases and Host Defense, Gunma University Graduate School of  
16 Medicine, Maebashi, Gunma, Japan

17 <sup>6</sup>Virus Vaccine Group, BIKEN Innovative Vaccine Research Alliance Laboratories, Research institute  
18 for Microbial Diseases, Osaka University, Suita, Osaka, Japan

19 <sup>7</sup>These authors contributed equally.

20 <sup>8</sup>Lead Contact

21 \*Correspondence to: [hebina@biken.osaka-u.ac.jp](mailto:hebina@biken.osaka-u.ac.jp)

22  
23 **SUMMARY**

24 Live-attenuated vaccines are generally highly effective. Here, we aimed to develop one  
25 against SARS-CoV-2, based on the identification of three types of temperature-sensitive  
26 (TS) strains with mutations in nonstructural proteins (nsp), impaired proliferation at 37-  
27 39°C, and the capacity to induce protective immunity in Syrian hamsters. To develop a live-  
28 attenuated vaccine, we generated a virus that combined all these TS-associated mutations  
29 (rTS-all), which showed a robust TS phenotype *in vitro* and high attenuation *in vivo*. The  
30 vaccine induced an effective cross-reactive immune response and protected hamsters  
31 against homologous or heterologous viral challenges. Importantly, rTS-all rarely reverted to  
32 the wild-type phenotype. By combining these mutations with an Omicron spike protein to  
33 construct a recombinant virus, protection against the Omicron strain was obtained. We  
34 show that immediate and effective live-attenuated vaccine candidates against SARS-CoV-2  
35 variants may be developed using rTS-all as a backbone to incorporate the spike protein of  
36 the variants.

37

38 **Keywords: SARS-CoV-2, live-attenuated vaccine, temperature-sensitive, nsp3, nsp14, nsp16,**  
39 **vaccine platform**

40

## 41 INTRODUCTION

42 The COVID-19 pandemic, caused by the pathogen SARS-CoV-2, has had a serious impact on public  
43 health, with more than 500 million infection cases and over six million deaths reported worldwide  
44 (ourworldindata.org). To prevent the spread of COVID-19, several adenovirus-vectored and mRNA  
45 vaccines encoding the viral spike (S) protein gene have been developed and are presently widely used.  
46 These vaccines have been reported to induce robust humoral and cellular immune responses (Folegatti  
47 et al., 2020; Jackson et al., 2020; Sahin et al., 2021); however, there are concerns regarding adverse  
48 reactions caused by these vaccines, such as thrombosis and fever. Furthermore, variants of concern  
49 (VOC), which bear several mutations in the S protein, continually arise and contribute to the evasion  
50 of the humoral immunity generated against the ancestral S protein (Baum et al., 2020; Edara et al.,  
51 2021; Wibmer et al., 2021). To increase the induction of neutralizing antibodies against VOCs, such  
52 as the SARS-CoV-2 Omicron variant, most countries have been encouraging a third, and even a fourth,  
53 vaccine dose as a booster. Nevertheless, the antibody response induced by these vaccines is not  
54 persistent, demanding the development of alternative vaccines of different modalities to better control  
55 the ongoing pandemic.

56 Traditional live-attenuated vaccines are highly effective and have been successfully used against  
57 various diseases, including varicella, measles, and rubella viruses. These vaccines were developed by  
58 heterogeneous adaptation, isolating mutant viruses that cannot propagate in human cells (Makino et  
59 al., 1970; Parks et al., 2001; Sasaki, 1974; Shishido and Ohtawara, 1976; Takahashi et al., 1974;  
60 Zimmerman et al., 2018), or by isolating temperature-sensitive (TS) viruses that cannot replicate at  
61 the physiological human body temperature (Komase et al., 2006; Okamoto et al., 2016). In addition,  
62 a live influenza virus vaccine was developed by reassortment of viruses generated from a cold-adapted  
63 donor virus with temperature sensitivity-related mutations in six vRNA segments (Maassab and Bryant,  
64 1999; Murphy and Coelingh, 2002). The attenuated phenotype of this virus was confirmed by its  
65 capacity to replicate at 25–33°C but not at 37°C (Cox and Dewhurst, 2015). Therefore, several groups  
66 have been developing live-attenuated vaccines against SARS-CoV-2. For example, Trimpert et al. and  
67 CODAGENIX are developing a codon-deoptimization strategy (Trimpert et al., 2021; Wang et al.,  
68 2021) and Seo et al. followed the cold-adaptation approach for isolating live-attenuated TS strains  
69 (Seo and Jang, 2020).

70 In this study, we obtained four TS SARS-CoV-2 strains from a clinical isolate by random  
71 mutagenesis. These strains exhibited low pathogenicity and protecting immunogenicity *in vivo*. We  
72 identified that mutations in *nsp3*, *nsp14*, and *nsp16* genes are associated with the TS phenotype, and

73 generated a highly effective and safe live-attenuated vaccine candidate by combining these TS-related  
74 mutations. Moreover, this candidate vaccine could be adjusted with an appropriate S protein to  
75 generate vaccines for specific VOCs. We believe that this live-attenuated vaccine candidate is a  
76 promising platform to control the spread of the COVID-19 pandemic.

## 77 78 **RESULTS**

### 79 **SARS-CoV-2 TS mutants show attenuated phenotype and induce protective immunity**

80 To isolate the TS strains of SARS-CoV-2, we generated a library of viruses containing random  
81 mutations from the clinical isolate B-1 virus (accession number: LC603286) (Figure S1A). In total,  
82 659 viral plaques were isolated from the library and screened. Vero cells were infected with all viral  
83 clones, cultured at 32 or 37°C, and monitored daily for cytopathic effects (CPE). During this process,  
84 we selected four TS strains that induced CPE at 32°C three days post-infection (dpi) but not at 37°C.  
85 To comprehensively analyze temperature sensitivity, we evaluated the growth kinetics of the isolated  
86 TS strains at 32, 34, and 37°C (Figures 1A and S1B). Under 32°C and 34°C culture conditions, all TS  
87 strains replicated comparably to the parent B-1 virus. However, at 37°C, the replication of all TS  
88 strains was relatively slower or smaller in scale than that of the parent strain. The growth of the H50-  
89 11 strain was delayed ( $p < 0.001$ , at day 1); however, its titer on day three was comparable to the viral  
90 titer of the B-1 virus on the same day ( $p = 0.5034$ ). The L50-33 and L50-40 strains slightly proliferated  
91 at 37°C, and the viral titers were less than  $10^4$  TCID<sub>50</sub>/mL, even at five dpi, and were  $10^4$  times lower  
92 than the maximum titer of the B-1 strain. Interestingly, the A50-18 strain showed a unique phenotype,  
93 as no infectious viruses were detected in the culture medium at 37°C (the TCID<sub>50</sub> was under the assay's  
94 limit of detection).

95 Next, we evaluated the pathogenicity of TS mutant strains in Syrian hamsters, which are widely  
96 used as a model for SARS-CoV-2 infection (Imai et al., 2020; Sia et al., 2020) (Figure 1B). Viral  
97 pathogenicity was monitored based on the changes in body weight after viral infection. Compared to  
98 the mock group, B-1-infected hamsters significantly decreased their body weight, with an approximate  
99 decrease of 15% at day six (Figure 1C). In contrast, no body weight loss was observed after infection  
100 with any of the tested TS strains. To determine the acute signs that can be observed after infection with  
101 the TS strains, B-1- or TS strain-infected Syrian hamsters were euthanized at three dpi, and lung tissue  
102 damage was evaluated. The lungs of the B-1-infected hamsters were heavier than those of the mock-  
103 or TS-infected hamsters (Figure S1C). Additionally, we observed apparent bleeding and destruction  
104 of the alveoli in the lungs of B-1-infected hamsters (Figure S1D). However, we did not observe evident  
105 critical tissue damage in the TS-infected hamsters. We also measured the amount of virus remaining  
106 in the nasal cavity and lungs at three dpi. The viral titer in the nasal wash specimens of the TS-infected  
107 hamsters was significantly lower than that of the B-1-infected hamsters (Figure 1D). The mean viral  
108 titers were  $2.25 \times 10^5$ ,  $2.84 \times 10^4$ ,  $2.42 \times 10^3$ ,  $3.57 \times 10^4$ , and  $2.14 \times 10^4$  PFU/mL in B-1-, A50-18-,

109 H50-11-, L50-33-, and L50-40-infected hamsters, respectively. In addition, the viral titer in the lungs  
110 of the TS-infected hamsters was approximately 100 times lower than that in the lungs of the B-1-  
111 infected group; the mean titers were  $1.87 \times 10^7$ ,  $3.98 \times 10^5$ ,  $1.26 \times 10^5$ ,  $7.25 \times 10^4$ , and  $1.66 \times 10^5$   
112 PFU/g in B-1-, A50-18-, H50-11, L50-33, and L50-40-infected hamsters, respectively (Figure 1E).  
113 These results suggest that the attenuated phenotype of the TS strains was due to impaired viral  
114 replication in the lungs. Moreover, to examine whether infection with the TS strains injures the nasal  
115 mucosa, we analyzed transverse cross-sections of the nasal cavity at three dpi (Figure 1F). In the “level  
116 1” section, the anterior sections of the nasal cavity, the mucosal damage observed in A50-18-infected  
117 hamsters was similar to that observed in B-1-infected hamsters (Figure 1G). However, in “level 2 and  
118 3” slices (medial and posterior sections, respectively), the tissue damage caused by A50-18 infection  
119 was milder than that caused by B-1 (Figure 1H), suggesting that intranasal infection with TS strains  
120 hardly injures the inner area of the nasal cavity.

121 To evaluate whether the attenuated TS strains could be used as live vaccines, we measured  
122 neutralizing titers in sera collected 20 days after the first infection (Figure 1B). The neutralizing  
123 antibody titer was <64, 512-1024, 256-512, 128-1024, 512-2048, and 1024-2048 in the sera of  
124 hamsters infected with the mock, B-1, A50-18, H50-11, L50-33, and L50-40 strains, respectively  
125 (Figure 1I). To assess the persistence of immunity against the TS strain, we performed a longitudinal  
126 analysis of hamsters after A50-18 infection (Figure S1E). Neutralizing antibody titers increased by  
127 week 4, and were relatively maintained for at least 16 weeks (Figure S1F). Median titer values were  
128 256, 2048, 724.1, 512, 256, 512, 181, and 256 at weeks 2, 4, 6, 8, 10, 12, 14, and 16, respectively.  
129 Additionally, to assess vaccine efficacy, immunized Syrian hamsters were reinfected with the wild-  
130 type B-1 virus 21 days after the first infection (Figure 1B). No significant body weight decrease was  
131 observed in hamsters pre-infected with B-1 or TS strains, whereas primary B-1 strain infection resulted  
132 in noticeable body weight loss in naïve hamsters ( $p < 0.001$ , all groups, days 3 to 9, compared to naïve  
133 group) (Figure 1J), suggesting the induction of protective immunity. These results indicate that the  
134 four attenuated TS strains can be used as live vaccines.

135

### 136 **The substitutions *nsp3* 445F, *nsp14* 248V plus 416S, and *nsp16* 67I are crucial for the TS** 137 **phenotype**

138 We then performed a deep sequencing analysis to identify mutations in the four TS strains (Table  
139 1). The A50-18 strain had six missense mutations in the genes encoding *nsp14*, S, envelope (E), and  
140 nucleocapsid (N) proteins. The H50-11 strain had four missense mutations in the *nsp3*, *nsp16*, and  
141 *spike* genes. There were two missense mutations in the *nsp3* gene of the L50-33 strain and three  
142 missense mutations in the *nsp3* and *spike* genes of the L50-40 strains. The H50-18, L50-33, and L50-  
143 40 strains had a common deletion in *orf7a-orf8* (27549-28251).

144 To identify TS-related mutations in these TS strains, we sought to obtain revertants of these viruses

145 that can proliferate under high-temperature conditions (37-39°C). Vero cells were infected with each  
146 of the TS strains at a high multiplicity of infection (MOI; MOI= 1.0) and incubated at 37, 38, or 39°C.  
147 For the A50-18 strain, the number of CPE-positive wells was 19 out of 230 analyzed wells at 37°C  
148 and 5 out of 223 wells at 38°C. Sequencing analysis revealed that A50-18 revertants replaced the 248V  
149 or 416S substitutions in nsp14 with the wild-type sequence (248G or 416G) but not the other amino  
150 acid substitutions (Table 2). Additionally, these revertant viruses proliferated at high temperatures  
151 when either of the two substitutions returned to the wild-type amino acid, indicating that the  
152 substitutions nsp14 248V and 416G are coordinately involved in the TS phenotype. We compared the  
153 predicted crystal structures of A50-18 nsp14 to those of B-1 using Alphafold2 (Jumper et al., 2021).  
154 The model suggested that both 248V and 416S are located near the zinc finger2 domain, which has  
155 been reported to be important for enzymatic activity (Figure S2A). The 248V substitution prevented  
156 the formation of one hydrogen bond, whereas 416S altered the angle of the other. We obtained H50-  
157 11 revertants in 2/230 wells at 37°C and in 1/230 wells at 38°C. In these viruses, the nsp16 67I  
158 substitution was changed to the wild-type amino acid (67V) (Table 2). The crystal structure models  
159 predicted that the V67I substitution did not significantly affect the structure of nsp16 (Figure S2B).  
160 L50-33 revertants were obtained in 34/230 wells at 37°C, 39/228 wells at 38°C, and 13/230 wells at  
161 39°C. L50-40 revertants were obtained in 17/230 wells at 37°C, 14/228 wells at 38°C, and 4/216 wells  
162 at 39°C (Table 2). The number of wells that produced L50 revertant viruses was higher than that for  
163 the A50-18 and H50-11 strains. In the revertants of L50-33 and L50-40, nsp3 445F changed back to  
164 the wild-type amino acid (leucine) as expected, or was altered to either cysteine, valine, or isoleucine  
165 (Table 2). Taken together, these results suggest that nsp14 248V plus 416S, nsp3 445F, and nsp16 67I  
166 are responsible for the TS phenotype of each strain.

167

### 168 **The phenotype and attenuation of the TS strains are attributed to the substitutions nsp14 248V** 169 **plus 416S, nsp3 445F, and nsp16 67I**

170 To confirm the role of the identified substitutions in the TS phenotype, we constructed recombinant  
171 viruses using a circular polymerase extension reaction (Torii et al., 2021) (Figure 2A). Recombinant  
172 viruses bearing the 248V and/or the 416S substitutions in the nsp14 protein (r14<sub>248V</sub>, r14<sub>416S</sub>, r14<sub>248V</sub>,  
173 <sub>416S</sub>, respectively), the 67I substitution in the nsp16 (r16<sub>67I</sub>), the 445F substitution in the nsp3 (r3<sub>445F</sub>),  
174 and the deletion in the orf7a-orf8 (rΔORF7a-8) were generated. *In vitro* growth kinetics (Figure 2B)  
175 and *in vivo* pathogenicity (Figures 2C and 2D) of the viruses were compared. Under the 32°C culture  
176 condition, all recombinant mutants (r3<sub>445F</sub>, r16<sub>67I</sub>, r14<sub>248V</sub>, r14<sub>416S</sub>, r14<sub>248V</sub>, <sub>416S</sub>, and rΔORF7a-8)  
177 replicated comparably to the recombinant B-1 (rB-1) strain (Figure 2B). The r14<sub>248V</sub> and r14<sub>416S</sub>  
178 mutants proliferated comparably to rB-1 at 37°C, whereas r14<sub>248V</sub>, <sub>416S</sub> showed relatively slower growth  
179 at 37°C ( $p < 0.001$ , at day 1, compared to rB-1), and this difference was more pronounced at 39°C.  
180 The replication of r14<sub>248V</sub>, <sub>416S</sub> was not detected at 39°C (the TCID<sub>50</sub> was under the assay's limit of

181 detection), whereas that of r14<sub>248V</sub> was slightly delayed ( $p < 0.1$ , at day 1, compared to rB-1). In  
182 contrast, the replication of r14<sub>416S</sub> was not affected at 39°C. These results suggest that a double amino  
183 acid substitution in nsp14 (248V and 416S) is necessary for a stronger TS phenotype, which can be  
184 observed at 37°C. The proliferation of the r3<sub>445F</sub> virus was relatively slower or smaller in scale than  
185 that of rB-1 at 37°C ( $p < 0.01$ , at day 1). Moreover, at 39°C, the replication of these mutants was not  
186 detected (the TCID<sub>50</sub> was under the assay's limit of detection), indicating that the 445F substitution in  
187 nsp3 is responsible for the TS phenotype. The r16<sub>67I</sub> virus proliferated comparably to rB-1 at 37°C;  
188 however, the peak in viral growth at 39°C was delayed two days compared to that of rB-1. These  
189 results suggest that the 67I substitution in nsp16 is responsible for the TS phenotype. Similarly,  
190 replication of rΔORF7a-8, which is a recombinant mutant with a deletion in *orf7a-orf8* common to  
191 H50-11, L50-33, and L50-40, was delayed two days compared to that of rB-1 at 39°C. This result  
192 suggests that this deletion negligibly accounts for the TS phenotype. The A50-18 strain has an A504V  
193 substitution in nsp14 in addition to G248V and G416S. This triple amino acid substitution impaired  
194 plaque formation at 37°C, even at day 6 (Figure S3), suggesting that nsp14 504V is also involved in  
195 temperature sensitivity, although it is unnecessary.

196 Next, we assessed whether these recombinant TS mutants were as attenuated *in vivo* as the isolated  
197 parental TS strains, using Syrian hamsters (Figure 2C). A significant decrease in body weight of  
198 approximately 15% was observed at six dpi in rB-1-infected hamsters ( $p < 0.0001$ , compared to the  
199 mock group) (Figure 2D). In contrast, no body weight loss was observed after infection with the r3<sub>445F</sub>  
200 or r14<sub>248V, 416S</sub> viruses ( $p > 0.9999$  and  $p > 0.9999$ , respectively, at day 6, compared to the mock group).  
201 The r14<sub>248V-</sub>, r14<sub>416S-</sub>, and r16<sub>67I-</sub>infected groups showed a decrease in body weight of approximately  
202 10%; however, it was slightly less than that observed in the rB-1-infected group ( $p = 0.3308$ ,  $p =$   
203  $0.6894$ , and  $p = 0.1592$ , respectively, at day 6, compared with rB-1-infected group). The rΔORF7a-8-  
204 infected group lost as much weight as the rB-1-infected group did. Therefore, considering the *in vitro*  
205 growth kinetics data, the temperature sensitivity of the mutants was consistent with their level of  
206 attenuation.

207

### 208 **The rTS-all vaccine candidate strain is highly attenuated and shows high immunogenicity in** 209 **Syrian hamsters**

210 As described above, the TS-associated substitutions changed back to the wild-type amino acid when  
211 the virus was found to proliferate at high temperatures (Table 2). Moreover, hamsters infected with  
212 the L50-33 revertant exhibited a decrease of approximately 21% in body weight at six dpi (Figure  
213 S4A), suggesting a risk of virulent reversion if TS strains are used as vaccines. To decrease the risk of  
214 virulent reversion and to generate a safe vaccine candidate, we combined the TS-associated mutations  
215 of *nsp3*, *nsp14*, *nsp16*, and *Δorf7a-orf8*, whose mechanisms were predicted to be independent of one  
216 another (rTS-all). Thus, these mutations may act in synergy or complement each other, rendering a

217 more stable TS phenotype. To assess the reversion risk of rTS-all, we performed the experiment  
218 described in Figure 3A. Each TS virus was transferred to 39°C culture conditions, a non-permissive  
219 temperature, after an incubation period of one or two days at 32°C. Three days after passaging, we  
220 counted the number of CPE-positive wells and checked the genomic sequence of the TS-responsible  
221 substitutions of viruses in these wells. Replication of the B-1 strain was observed in all wells (Figure  
222 3B). In contrast, no CPE-positive wells were detected in the rTS-all-inoculated wells, whereas several  
223 revertants were detected in the isolated TS strains (A50-18, H50-11, and L50-33). Moreover, to  
224 confirm whether the rTS-all reverts its amino acid substitution and recovers its virulence *in vivo*,  
225 hamsters were infected with rTS-all or L50-33 strains, and the genomic viral sequences and titers in  
226 nasal wash specimens were analyzed (Figure S4B). Although none of the infected hamsters lost weight  
227 (Figure S4C), the virus titer in nasal wash specimens of L50-33-infected hamsters were higher than  
228 that of rTS-all-infected hamsters (Figure S4D). Consistently, these viruses showed sequence  
229 alterations encoding for most probably leucine or cysteine at position 445 in nsp3, showing no TS  
230 phenotype (Figure S4D, Table 2). In contrast, rTS-all didn't show changes in any of the TS mutations,  
231 in three independent experiments (Figure S4E). These results suggest that the risk of virulent  
232 reversion of rTS-all might be lower than that of the isolated TS strains. Furthermore, the *in vitro* growth  
233 kinetic assays demonstrated that the replication of rTS-all was impaired under 37°C and 39°C culture  
234 conditions (Figure 3C). Even at 32°C, rTS-all started to proliferate later than rB-1, at one dpi ( $p <$   
235 0.0001). These results suggest that rTS-all is highly sensitive to temperature.

236 To investigate the *in vivo* levels of attenuation and immunogenicity, Syrian hamsters were first  
237 inoculated intranasally with  $1.8 \times 10^5$  TCID<sub>50</sub>/100  $\mu$ L/dose of rB-1 or rTS-all and reinfected with the  
238 wild-type B-1 virus 21 days later (Figure 3D). No body weight loss was observed after primary  
239 infection with rTS-all; however, the body weight of the rB-1-infected group decreased by  
240 approximately 15%, suggesting that rTS-all was indeed attenuated (Figure 3E). Moreover, the viral  
241 titer in the lungs of rTS-all-infected hamsters was remarkably lower than that in the lungs of rB-1-  
242 infected hamsters, with mean viral titers of  $6.29 \times 10^7$  and  $3.08 \times 10^3$  PFU/g in rB-1- and rTS-all-  
243 infected hamsters, respectively (Figure 3F). The viral titer in nasal wash specimens of rTS-all-infected  
244 hamsters was also markedly lower than that of rB-1-infected hamsters, with mean viral titers of  $1.01$   
245  $\times 10^5$  and  $1.39 \times 10^4$  PFU/mL in rB-1- and rTS-all-infected hamsters, respectively (Figure 3G). These  
246 results indicated that rTS-all is a hyper-attenuated mutant as its replication in the lungs is greatly  
247 impaired.

248 The titer of neutralizing antibodies in the serum of mock-infected hamsters was  $<64$  (Fig. 3H), and  
249 it was not significantly different between the rTS-all-infected group and the rB-1-infected group,  
250 ranges being 128-1024 (vs B-1), 64-512 (vs Gamma strain: hCoV-19/Japan/TY7-501/2021), 256-1024  
251 (vs Delta strain: BK325), respectively. These results suggest that the humoral immune responses  
252 induced by infection with the attenuated rTS-all was comparable to that induced by rB-1, even against

253 heterologous virus infection. Importantly, no significant weight decrease was observed after  
254 challenging hamsters pre-infected with rB-1 or rTS-all with the B-1 virus (Figure 3I), suggesting that  
255 infection with rTS-all induced protective immunity.

256

### 257 **Live-attenuated TS viruses are effective against the variant Omicron**

258 Antigenic drift has enabled Omicron, the latest VOC, to propagate around the world and become  
259 dominant in one month (CDC). To evaluate whether rTS-all-infection protects against the Omicron  
260 variant, Syrian hamsters were inoculated intranasally with  $1.8 \times 10^5$  TCID<sub>50</sub>/100  $\mu$ L/dose of rB-1 or  
261 rTS-all. Inoculation with rB-1 and rTS-all induced neutralizing antibodies against the homologous  
262 virus B-1 (Figure 4B). Furthermore, titers against the Omicron variant were <32-128 in hamsters  
263 infected with rB-1 or rTS-all (Figure 4C). To evaluate whether rTS-all induces heterologous protection,  
264 animals were challenged with the TY38-873 Omicron virus ( $7.2 \times 10^4$  TCID<sub>50</sub>/20  $\mu$ L) 28 days after  
265 the initial inoculation (n = 5, Figure 4A). Viral titers in the lungs and nasal specimens, collected three  
266 days after Omicron infection, were measured by plaque assays. In the lungs, the mean viral titer in the  
267 rB-1- and rTS-all-infected groups was significantly lower than that in the mock-infected group, which  
268 had a titer of  $6.4 \times 10^5$  PFU/g (Figure 4D). The mean viral titer in nasal wash specimens of the rB-1-  
269 and rTS-all-infected groups was remarkably lower than that of the mock-infected group ( $5.2 \times 10^3$   
270 PFU/mL; Figure 4E). Additionally, the titers in the lungs and nasal wash of the rB-1- and rTS-all-  
271 infected groups were not significantly different, suggesting that rTS-all infection can protect hamsters  
272 from an Omicron infection, as well as the wild-type infection, by inducing cross-reactive neutralizing  
273 antibodies. Moreover, we compared the neutralizing antibody titers in the nasal wash specimens of the  
274 rB-1- and rTS-all-infected groups, collected 28 days after primary infection, using a VSV $\Delta$ G/Luc-  
275 encoding SARS-CoV-2 S-expressing pseudovirus (Tani et al., 2010). The nasal wash specimens of the  
276 rTS-all-infected group showed significantly lower luciferase activity than that of the mock group,  
277 similar to the rB-1-infected group (Figure 4F). This result suggests that infection of the nasal mucosa  
278 with rTS-all can induce neutralizing antibodies to protect against viral entry. Collectively, these data  
279 demonstrate that infection with rTS-all induces the production of systemic and mucosal neutralizing  
280 antibodies, which can prevent infection with heterologous viruses, similar to the wild-type infection.

281

### 282 **A strategy based on TS-associated mutations and adjusted with tailor-made S proteins to target** 283 **different variants**

284 The identified TS substitutions were located in the viral nsps and did not affect the antigenicity of  
285 the S proteins. Thus, we hypothesized that we could design a vaccine platform against VOCs by  
286 exchanging the S protein of rTS-all with that of the other strains. To confirm this hypothesis, we  
287 constructed a recombinant virus (rTS-all-Omicron) containing the coding sequence of the Omicron S  
288 protein within the TS-all backbone (Figure 5A). As expected, rTS-all-Omicron exhibited a TS

289 phenotype *in vitro* (Figure 5B). Furthermore, to evaluate its efficacy as a vaccine against Omicron, we  
290 measured the titer of neutralizing antibodies in the serum of hamsters 14 days after infection (Figure  
291 5 C). Consistent with our findings in Figure 4C, the titer against Omicron in the rTS-all-infected group  
292 was low (<32 at 14 dpi). However, infection with the rTS-all-Omicron significantly increased the titer  
293 of neutralizing antibodies against Omicron (128-256) but not that against the B-1 strain (<32), which  
294 has the D614G S protein (Figure 5D). These results confirmed that vaccination with rTS-all-Omicron  
295 is effective at protecting against Omicron, suggesting the possibility that rTS-all constitutes a powerful  
296 platform for the development of a COVID-19 live-attenuated vaccine by replacing the spike protein  
297 with that of newly emerging variants.

298

## 299 DISCUSSION

300

301 Live-attenuated viruses constitute a highly effective vaccine modality that has been used to treat  
302 various infectious diseases. They have several advantages including the induction of an effective  
303 humoral immune response and a long-lasting protective cellular immunity without the need for  
304 multiple doses. However, there are concerns regarding virulence reversion, such as that reported for  
305 oral poliovirus vaccines (Kew et al., 2005). In this study, we identified TS-associated mutations in  
306 several SARS-CoV-2 nsps that resulted in TS phenotypes of varying degrees of *in vitro* and *in vivo*  
307 attenuation in the Syrian hamster model (Figures 1 and S1B- D). To develop a safe and effective live-  
308 attenuated vaccine, we hypothesized that combining all these mutations may lead to a virus that is less  
309 likely to revert to the more pathogenic wild-type phenotype. Thus, we generated a recombinant virus,  
310 rTS-all, and confirmed that it retained TS characteristics *in vitro* and *in vivo*. More importantly, the  
311 generation of revertants proved to be less likely in comparison, both *in vitro* and *in vivo*, strengthening  
312 the potential use of rTS-all as a vaccine against COVID-19 (Figure 3, S4).

313 One of the identified mutations resulted in a V67I substitution within the viral nsp16 protein, which  
314 is a 2-O-methyltransferase involved in viral genome replication (Chen et al., 2011; Decroly et al.,  
315 2011; Decroly et al., 2008; Krafcikova et al., 2020). Structural analyses (AlphaFold2; Figure S2B)  
316 (Jumper et al., 2021) of this protein predicted no drastic differences compared with the wild-type  
317 version, consistent with the weak phenotype of the strain (H50-11). Another substitution was found in  
318 the MACS domain of nsp3 (L445F), accounting for the modest TS phenotypes of the L50-33 and L50-  
319 40 strains. In mouse hepatitis virus (MHV), mutations in the nsp3 MAC domain can cause temperature  
320 sensitivity, likely by enhancing proteasome-mediated degradation (Deng et al., 2019). Therefore, we  
321 speculated that the mechanisms underlying the TS phenotype in our isolated strains might be similar.  
322 Finally, several substitutions were identified in nsp14 (G248V, G416S, and A504V), rendering the  
323 resulting A50-18 strain more sensitive to higher temperatures. The predicted structure model suggested  
324 that both 248V and 416S substitutions affected hydrogen bonds (Figure S2A). The nsp14 protein has

325 exo-ribonuclease and N7 methyltransferase domains and plays an important role in viral genome  
326 replication by forming a complex with other nsps (Chen et al., 2009; Minskaia et al., 2006; Ogando et  
327 al., 2020). Therefore, at high temperatures, these structural changes may affect the molecular  
328 interactions within nsp14 itself and with other nsps, resulting in a decline in viral genome replication.

329 The strain, rTS-all, which combines all the above mutations, exhibited an attenuated phenotype  
330 while maintaining robust immunogenicity *in vivo* (Figure 3). Infection with rTS-all induced serum  
331 neutralizing antibodies against not only the homologous virus but also heterologous viruses, that were  
332 comparable to those induced by rB-1 infection (Figures 3H, 4 B, and 4C). These results are most likely  
333 due to a more complex immunization process. Despite attenuation, the infecting virus stimulates  
334 several pathways of the immune system throughout its cycle within the infected cells (Shah et al.,  
335 2020), which might induce a highly effective immune response. A previous study has suggested that  
336 infection-induced primary memory B cells undergo more affinity maturation than vaccine-induced  
337 memory B cells do (Pape et al., 2021). Therefore, rTS-all infection may also induce mature B cells.

338 A previous study has reported that mucosal IgA against SARS-CoV-2 is present in convalescent  
339 patients and contributes to virus neutralization (Sterlin et al., 2021). However, it is not induced after  
340 vaccination with mRNA through the intramuscular route (Piano Mortari et al., 2021). An animal model  
341 study has reported that vaccination-induced systemic neutralizing antibodies failed to protect nasal  
342 tissue against SARS-CoV-2 infection (Zhou et al., 2021). Consistent with these studies, in the present  
343 study, we observed that intranasal administration of live-attenuated rTS-all induced neutralizing  
344 antibodies not only in the serum but also in the nasal mucosa, similar to the wild-type infection  
345 (Figures 4B, 4C, and 4F). Moreover, rTS-all-infected animals were protected from not only the B-1  
346 strain but also the Omicron variant (Figures 3I, 4D, and 4E). We speculate that mucosal neutralizing  
347 antibodies induced by rTS-all intranasal administration might play an important role in protection  
348 against SARS-CoV-2 in peripheral areas.

349 A serious concern related to intranasal administration of live viruses is olfactory dysfunction, which  
350 has been reported after infection with SARS-CoV-2 (Giacomelli et al., 2020), probably as a  
351 consequence of nasal tissue damage (Khan et al., 2021; Urata et al., 2021). In this study, we confirmed  
352 that infection with A50-18 resulted in dramatically lower damage to the nasal tissue compared to  
353 infection with the wild-type strain. Therefore, our data suggest that the intranasal administration of  
354 rTS-all might constitute a safe option for the development of an effective vaccine strategy for  
355 protection against SARS-CoV-2 infections.

356 Previous studies have suggested that SARS-CoV-2 induces a broad, robust, and specific T-cell  
357 response in convalescent individuals (Grifoni et al., 2020; Sekine et al., 2020). In our study, rTS-all  
358 exhibited a lower proliferation rate than the wild-type virus in the lungs, as well as less pathogenicity  
359 (Figure 3F). However, it replicated in the nasal cavity, which is a low-temperature region (Figure 3G).  
360 Although we did not assess cellular immunity in this study, infection with the rTS-all strain might

361 elicit a T-cell response similar to that of the wild-type strain.

362 Our study also offers a strong vaccine platform applicable to future variants. As nsp3, nsp14, and  
363 nsp16 do not affect the antigenicity of the S protein, alternative TS strains can be generated by  
364 changing the S coding sequence. Here, we confirmed that rTS-all-Omicron exhibited immunogenicity  
365 against the Omicron variant and conserved the TS phenotype characteristics of the original rTS-all  
366 strain.

367 Several live-attenuated vaccines have been reported in previous studies that were developed  
368 following different strategies. Ye et al. reported that a nsp16-deficient strain with a single point  
369 mutation (d16) was stable for 10 passages in Vero E6 cells (Ye et al., 2022). We have observed that  
370 the combination of several mutations renders rTS-all less prone to virulent reversion, both *in vitro* and  
371 *in vivo*, compared to single ones (Figure 3B, S4D). Therefore, we consider that rTS-all is a safer  
372 candidate for a live-attenuated vaccine. Another approach, cold-adaptation of virus was performed by  
373 Seo and Jang (Seo and Jang, 2020). This virus contained 11 unique amino acid substitutions, three of  
374 which were present in the Spike protein, but the phenotype responsible mutations were not  
375 characterized in detail. Codon deoptimization of the spike coding sequence was attempted by Trimpert  
376 et al. and CODAGENIX (Trimpert et al., 2021; Wang et al., 2021). Compared with these strains, the  
377 advantage of the attenuated phenotype of the rTS-all strain lies in the amino acid substitutions outside  
378 of the spike protein, which is what varies the most among virus strains and which mainly shapes the  
379 protective immune response. Thus, it might constitute a suitable and versatile backbone where to insert  
380 spike proteins of emerging VOCs. Notably, we were able to generate the rTS-all-Omicron virus two  
381 weeks after the Omicron sequence was made available. Unlike the live-attenuated strains as mentioned  
382 above, the rTS-all strain has impaired replication at 37°C and conserves an immunogenicity  
383 comparable to the wild type strain, based on its proliferation in the anterior regions of the nasal cavity,  
384 as was observed for the A50-18 strain (Figure 1G, 1H). Therefore, we believe that rTS-all might be  
385 less likely to damage the olfactory epithelium. Moreover, from the production point of view, rTS-all  
386 shows normal replication at 32°C, which makes its amplification at manufacturing scales easily  
387 achievable, also reported by Seo and Jang, Trimpert et al. and Wang et al.. Overall, our data suggest  
388 that this platform could be a promising candidate for the development of a live-attenuated vaccine that  
389 can be rapidly produced in response to new emerging variants or another SARS-CoV pandemic in the  
390 future.

391

392 Limitations of the study

393 Detailed characterization of the cellular and humoral immune responses was difficult using this model,  
394 due to the lack of hamster-specific reagents. Using a genetically modified mouse model could help  
395 circumvent this problem. Furthermore, it is unclear whether virulent reversion occurs during *in vivo*  
396 transmission, thus additional studies are required. In addition, olfactory functional analysis could help

397 better determine its correlation with the nasal tissue injury, an important point for the development of  
398 intranasal attenuated vaccines.

399

#### 400 **ACKNOWLEDGMENTS**

401 We appreciate the assistance from Mitsuyo Kosaka, Mai Matsumoto, and Manae Morishima (BIKEN).  
402 The authors acknowledge the NGS core facility of the Genome Information Research Center at the  
403 Research Institute for Microbial Diseases of Osaka University for their support with next generation  
404 sequencing analyses. This work was supported by The Research Foundation for Microbial Diseases  
405 of Osaka University (BIKEN) and Japan Agency for Medical Research and Development (AMED)  
406 under Grant Number JP20pc0101047.

407

#### 408 **AUTHOR CONTRIBUTIONS**

409 H.E. conceived and designed the study. A.Y. and S.O. conducted the majority of the experiments. S.T.,  
410 C.O., and Y.M. constructed the CPER fragments for the construction of recombinant viruses. S.K.  
411 performed the pseudovirus neutralization assays. Hitomi S. performed the experiments related to the  
412 longitudinal evaluation of the immune response. Hidehiko S., S.U., and W.K. provided scientific  
413 insight. A.Y., S.O., and P.M. wrote the original manuscript and H.E. revised it. S.T., K.Y., and H.E.  
414 supervised the project.

415

#### 416 **DECLARATION OF INTERESTS**

417 A.Y., S.O., S.K., Hitomi S., Hidehiko S., P.M., S.T., K.Y., and H.E. are employed by BIKEN. We  
418 report that A.Y., S.O., and H.E. are named on a patent that describes the use of the TS mutants as  
419 vaccines, currently being filed by BIKEN. Shiro T. and H.E are managers of BIKEN. K.Y is the  
420 director general of BIKEN. Shiho T., C.O., Y.M., S.U., and W.K. have no conflict of interests to  
421 declare.

422

#### 423 **FIGURE LEGENDS**

##### 424 **Figure 1. SARS-CoV-2 TS mutants show attenuated phenotype and induce protective immunity**

425 (A) Comparison of the growth kinetics of the four TS mutants with those of the B-1 strain at different  
426 temperatures. Vero cells were infected with each strain at multiplicity of infection (MOI) = 0.01. The  
427 viral titer of the supernatant was evaluated by TCID<sub>50</sub> using Vero cells. Symbols represent the average  
428 of three independent experiments, and error bars depict the mean SDs. For samples below the limit of  
429 detection (LOD), the assay's LOD was used to calculate the mean. The LOD is 2.05 log<sub>10</sub> TCID<sub>50</sub>/mL,  
430 indicated in the x-axis. TCID<sub>50</sub>: 50% tissue culture infectious dose. To compare titers on the same day  
431 between the B-1 and the other strains, two-way ANOVA was performed.

432 (B) Overview of the evaluation for pathogenicity and immunogenicity of TS mutants (n = 5).

433 (C) Weight changes in the Syrian hamsters infected with the TS mutant or B-1 strains. The average  
434 weight change is plotted, and error bars represent the SDs. To compare weight change on the same  
435 day between the mock and the other groups, two-way ANOVA was performed (\*\*p < 0.01 and \*\*\*\*p  
436 < 0.0001).

437 (D, E) The viral titers of nasal wash specimens (D) and lung homogenates (E) three days post-infection.  
438 Infectious viruses were evaluated by plaque formation assays. PFU: plaque-forming units. Bars depict  
439 the mean values, and symbols represent individual viral titers. Error bars represent SDs. For statistical  
440 analysis, one-way ANOVA was performed (\*\*p < 0.01 and \*\*\*p < 0.001).

441 (F) Schematic diagram for the evaluation of mucosal tissue damage (n = 4).

442 (G) Damage scores of each section. The percentage of the disrupted area in the entire visual field was  
443 classified as 0: not remarkable (< 10%), 1: minimal (10-50%), and 2: mild (50-70%) respectively.

444 (H) Representative hematoxylin and eosin (HE)-stained images of sections at level 3. Scale bar: 1000  
445  $\mu\text{m}$  (left panel), and 200  $\mu\text{m}$  (right panel). Right panels are higher magnification images of the marked  
446 areas.

447 (I) Neutralization titers of the sera from hamsters infected with each strain and mock-treated hamsters.  
448 Median values are plotted, and error bars represent the 95% CIs. For statistical analysis, the Kruskal-  
449 Wallis test was performed (n.s.: not significant). The LOD is indicated in the x-axis.

450 (J) Weight change in hamsters after B-1 virus reinfection. The average weight change is plotted, and  
451 error bars represent mean SDs. To compare weight change on the same day between the naïve and the  
452 other groups, two-way ANOVA was performed.

453

454 **Figure 2. The phenotype and attenuation of the TS strains are attributed to the substitutions**  
455 **nsp14 248V plus 416S, nsp3 445F, and nsp16 67I**

456 (A) The construct of recombinant viruses bearing the substitutions or the deletion found in the TS  
457 strains.

458 (B) The growth kinetics of recombinant viruses at different temperatures. Vero cells were infected with  
459 each strain at MOI = 0.01. The viral titer of the supernatant was calculated by TCID<sub>50</sub> using Vero cells.  
460 Symbols represent the average of three independent experiments, and error bars mean SDs. For  
461 samples below the LOD, the assay's LOD was used to calculate the mean. The LOD is 2.65 log<sub>10</sub>  
462 TCID<sub>50</sub>/mL, indicated in the x-axis. To compare titers on the same day between the B-1 and the other  
463 strains, two-way ANOVA was performed.

464 (C) Evaluation of the pathogenicity of recombinant viruses *in vivo* (n = 5).

465 (D) Weight change in the Syrian hamsters infected with the recombinant viruses. The average weight  
466 changes are represented by symbols, and SDs are represented by error bars. For statistical analysis,  
467 two-way ANOVA was performed.

468

469 **Figure 3. The rTS-all vaccine candidate strain is highly attenuated and shows high**  
 470 **immunogenicity in Syrian hamsters**

471 (A) Scheme for the evaluation of the risk of virulent reversion by their ability to replicate at lower  
 472 temperatures.

473 (B) The number of CPE-positive wells (upper line) and that of those that changed back to the wild-  
 474 type sequence (lower line).

475 (C) Growth dynamics of the rTS-all and rB-1 strains at different temperatures. Vero cells were infected  
 476 with each strain at MOI = 0.01. Infectious viruses in the supernatants were evaluated by TCID<sub>50</sub> in  
 477 Vero cells. Symbols represent the average of three independent experiments, and error bars represent  
 478 SDs. For samples below the LOD, the assay's LOD was used to calculate the mean. The LOD is 2.65  
 479 log<sub>10</sub> TCID<sub>50</sub>/mL, indicated in the x-axis. For statistical analysis, two-way ANOVA was performed  
 480 (\*p<0.05 , \*\*\*\*p<0.0001).

481 (D) Overview of the investigation of the pathogenicity and immunogenicity of the rTS-all strain (n =  
 482 5).

483 (E) Weight change in the recombinant viruses-infected hamsters. The average weight change is plotted,  
 484 and error bars represent the SDs. For statistical analysis, two-way ANOVA was performed  
 485 (\*\*\*\*p<0.0001).

486 (F, G) The viral titers in lung homogenates (F) and nasal wash specimens (G) three days post-infection.  
 487 Viral titration was performed by plaque formation assays. Bars depict the mean values, and symbols  
 488 represent individual viral titers. Error bars represent mean SDs. The LOD is indicated in the x-axis.  
 489 For statistical analysis, one-way ANOVA was performed (\*\*p < 0.01 and \*\*\*p < 0.001).

490 (H) Neutralization titers in the sera of rB-1 or rTS-all-infected and mock-treated hamsters. Symbols  
 491 represent individual neutralization titers. Bars show median values and error bars represent 95% CIs.  
 492 For statistical analysis, the Kruskal-Wallis test was performed (n.s.: not significant). The LOD is  
 493 indicated in the x-axis.

494 (I) Weight change in Syrian hamsters after reinfection with the B-1 virus. The average weight change  
 495 is plotted, and error bars represent mean SDs. To compare weight change on the same day between  
 496 the naïve and the other groups, two-way ANOVA was performed (\*p < 0.05, \*\*p < 0.01, and \*\*\*\*p <  
 497 0.0001).

498

499 **Figure 4. Live-attenuated TS viruses are effective against the variant Omicron**

500 (A) Evaluation of the immunogenicity the rTS-all strain *in vivo*.

501 (B, C) Neutralization titers in the sera of immunized hamsters against the B-1 (B) and BA.1 viruses

502 (C). Individual neutralization titers are plotted with symbols and bars showing the median values  
 503 (Mock and rTS-all; n = 10, rB-1; n = 9). Error bars represent 95% CIs. The LOD is indicated in the x-  
 504 axis. Kruskal-Wallis test was used for statistical analysis (n.s.: not significant, \*\*p < 0.01 and \*\*\*p <

505 0.001).  
506 (D, E) Viral titers in lung homogenates (D) and nasal wash specimens (E) three days post-infection.  
507 Viral titration was performed by plaque formation assays. Bars depict the mean values, and symbols  
508 represent individual viral titers (n = 5). Error bars represent mean SDs. The LOD is indicated in the x-  
509 axis. For statistical analysis, one-way ANOVA was performed (n.s.: not significant, \*p < 0.05, and  
510 \*\*\*\*p < 0.0001).

511 (F) Neutralization assay of the nasal wash specimens against pseudotyped VSV with D614G pre-alpha  
512 type spike. The symbols represent individual data and error bars represent SDs (Mock and rTS-all; n  
513 = 5, rB-1; n = 3). The data were statistically analyzed using one-way ANOVA (n.s.: not significant, \*p  
514 < 0.05 and \*\*p < 0.01).

515

516 **Figure 5. A strategy based on TS-associated mutations and adjusted with tailor-made S proteins**  
517 **to target different variants**

518 (A) The construct of recombinant viruses which contained the Omicron spike with all the substitutions  
519 or deletions involved in temperature sensitivity.

520 (B) Temperature sensitivity of rTS-all-Omicron *in vitro*. Vero cells were infected with the recombinant  
521 strains and the Omicron variant and incubated under the indicated temperature conditions. CPE were  
522 observed three dpi by formalin fixation and crystal violet staining.

523 (C) Evaluation of the immunogenicity of the rTS-all-Omicron strain *in vivo* (n = 5).

524 (D) Neutralization titer of the sera from the hamsters infected with each strain. The individual  
525 neutralization titers are indicated with the corresponding symbols. Bars represent median values and  
526 error bars mean 95% CIs. For statistical analysis, the Kruskal-Wallis test was performed (n.s.: not  
527 significant). The LOD is indicated in the x-axis.

528

**529 RESOURCE AVAILABILITY****530 Lead contact**

531 Further requests for resources and reagents should be directed to and will be fulfilled by the lead  
532 contact, Hiroataka Ebina (hebina@biken.osaka-u.ac.jp).

533

**534 Materials availability**

535 The principal authors of this paper are employees of the Research Foundation for Microbial Diseases  
536 of Osaka University (BIKEN). Therefore, the distribution of the TS strains and their composite strains  
537 obtained in this study requires the establishment of an MTA with BIKEN.

538

**539 Data and code availability**

540 The data in this report are available from the lead contact upon request. The viral genome sequences  
541 of the TS mutants isolated in this study have been deposited at the National Center for Biotechnology  
542 Information (Accession numbers 5 for B-1, A50-18, H50-11, L50-33 and L50-40 are LC603286,  
543 LC603287, LC603288, LC603289 and LC603290, respectively). All other data needed to evaluate the  
544 conclusions in the paper are present in the paper or the Supplemental information. Additional  
545 information for reanalysis is shared by the lead contact upon request.

546

**547 EXPERIMENTAL MODEL AND SUBJECT DETAILS****548 Ethical statement**

549 All animal experimental protocols, including anesthesia conditions, endpoints for infection, and  
550 euthanasia methods; and genetic recombination experiments, were reviewed and approved by the  
551 corresponding Osaka University's Review Committees (approval no. R02-10, approval no. 4680,  
552 respectively).

553

**554 Hamsters**

555 Male Syrian hamsters (SLC:Syrian, 4-weeks old) were purchased from Japan SLC, Inc (Shizuoka,  
556 Japan). Hamsters were housed under a 12-h light/12-h dark cycle and were allowed free access to food  
557 and water. Hamsters were used for each experiment after a 1-week adjustment period

558

**559 Cell lines**

560 Vero cells (African green monkey kidney cells: ATCC, CCL-81) and 293T cells (human embryonic  
561 kidney cells: ATCC, CRL-3216) were maintained at 37°C in Dulbecco's modified Eagle's Medium  
562 (DMEM, Sigma-Aldrich, Cat# D6429) supplemented with 10% heat-inactivated fetal bovine serum  
563 (FBS, Sigma-Aldrich), penicillin (100 U/mL), and streptomycin (0.1 mg/mL) (PS, Gibco, Cat#  
564 1154887). VeroE6-TMPRSS2 cells (TMPRSS2-expressing Vero cells: JCRB, JCRB1819) were

565 maintained at 37°C in DMEM supplemented with 10% heat-inactivated FBS, PS, and 1 mg/mL G418  
566 Sulfate (Gibco, Cat# 10131027). BHK cells (hamster kidney cells: JCRB, JCRB9020) were  
567 maintained at 37°C in Minimum Essential Medium Eagle (MEM, Sigma-Aldrich, Cat# M4655)  
568 supplemented with 10% heat-inactivated FBS and PS. BHK cells stably expressing human ACE2 were  
569 generated by piggyBac plasmid transfection and puromycin-based selection and maintained with 3  
570 µg/mL puromycin (Gibco, Cat# A1113803).

571

## 572 **Viruses**

573 SARS-CoV-2 was isolated from a SARS-CoV-2-positive clinical specimen in Osaka City, Japan. An  
574 aliquot of 500 µL of the specimen was diluted with 500 µL of Dulbecco's phosphate-buffered saline  
575 (D-PBS, Nacalai Tesque, Cat# 14249) and filtered through a 0.22 µm filter. One hundred microliters  
576 of this filtrate were used to inoculate the Vero cells. Cytopathic effects (CPE) were observed three  
577 days post-infection (dpi). The supernatant was collected and stored at -80°C as the "SARS-CoV-2  
578 clinical isolate strain B-1". Whole-genome sequencing of B-1 was performed using next-generation  
579 sequencing (NGS) analysis, as described below. The sequencing results showed that the B-1 strain had  
580 a D614G substitution in the S protein. The SARS-CoV-2 delta variant (BK325) was provided by the  
581 Research Foundation for Microbial Diseases of Osaka University. The gamma (hCoV-19/Japan/TY7-  
582 501/2021, GISAID ID: EPI\_ISL\_833366) and Omicron variants (TY38-873, GISAID ID:  
583 EPI\_ISL\_7418017) were obtained from the National Institute of Infectious Diseases of Japan (NIID).  
584 A pseudotyped vesicular stomatitis virus (VSV) with the SARS-CoV-2 S protein (pre-alpha type:  
585 D614G) was constructed for neutralization assays. The pCAGGS plasmid encoding the codon-  
586 optimized SARS-CoV-2 *spike* gene lacking the C-terminal 19 amino acids was transfected into 293T  
587 cells using polyethylenimine (Polysciences, Cat# 24765). Twenty-four hours post-transfection,  
588 VSVΔG/Luc-complemented VSV G pseudovirus, where the VSV G gene was replaced by the  
589 luciferase gene but expressed VSV G on the surface of the virion (VSVΔG/Luc complemented with  
590 VSV G), was used to infect cells at multiplicity of infection (MOI) = 0.1 (Tani et al., 2010). The excess  
591 unattached virus was eliminated by removing the supernatant two hours post-infection and replacing  
592 it with a fresh medium. After 72 h of incubation at 37°C, the cell culture supernatants containing  
593 VSVΔG/Luc-encoding SARS-CoV-2 S-expressing pseudovirus were collected and filtered through a  
594 0.45 µm pore size filter.

595

## 596 **Evaluation of pathogenicity in hamsters**

597 Syrian hamsters (Slc:Syrian) were purchased from Japan SLC, Inc. Five-week-old male hamsters were  
598 anesthetized with 2.0-3.0% isoflurane (FUJIFILM Wako, Cat# 1349003) inhalation and 0.3 mg/kg  
599 medetomidine (Nippon Zenyaku Kogyo) + 4 mg/kg midazolam (Maruishi Pharmaceutica) + 5 mg/kg  
600 butorphanol (Meiji Seika Pharma) intraperitoneal injection. One hundred microliters of DMEM

601 containing the respective SARS-CoV-2 strains were delivered dropwise to the nostrils, and body  
602 weight was measured daily. For the assessment of acute symptoms, lung and nasal wash specimens  
603 were collected with 1 mL of D-PBS at three dpi. The lungs were divided into left and four right lungs.  
604 The left lung was fixed with 10% formalin and serially sectioned. One section was stained with  
605 hematoxylin (Sakura Finetek Japan, Cat# 9130-4P) and eosin (FUJIFILM Wako, Cat# 051-06515).  
606 The right lung was homogenized with Biomasher II (Nippi, Cat# 320 103) and suspended in 1 mL of  
607 DMEM. After centrifugation at 100 g for 5 min, the supernatant was collected as lung homogenate.  
608 The viral titers of these samples were evaluated using a plaque formation assay. To evaluate the tissue  
609 damage in the nasal cavity caused by infection with the TS mutants, hamsters were infected with  
610 SARS-CoV-2 B-1 or A50-18 strains contained in 20  $\mu$ L of DMEM via the intranasal route to limit the  
611 administration to the upper respiratory tract. After euthanasia, the heads were fixed in 10% formalin  
612 and sectioned. Each section was stained with hematoxylin and eosin (HE).

613

#### 614 **Evaluation of antigenicity in hamsters**

615 To analyze antigenicity, we performed a re-challenge assay and evaluated the presence of neutralizing  
616 antibodies in the serum and nasal wash specimens. Hamsters who recovered from the SARS-CoV-2  
617 primary infection were re-challenged with DMEM containing the respective SARS-CoV-2 strains  
618 three weeks after the first infection. Body weight changes were recorded for an additional 8-10 d. For  
619 the neutralization assay, blood and nasal wash specimens were collected from the recovered hamsters.  
620 The blood specimens were centrifuged at 800 g for 10 min, and serum was collected for analysis.  
621 Nasal wash specimens were filter-sterilized prior to the assay.

622

## 623 **METHOD DETAILS**

### 624 **Plasmids**

625 The *hACE2* gene was cloned into the piggyBac plasmid (Systembiosciences, PB514B-2). Briefly, total  
626 RNA was extracted from 293T cells and reverse-transcribed using the SuperScript™ III First-Strand  
627 Synthesis System for RT-PCR (Invitrogen, Cat# 11904018). Then, hACE2 complementary DNA  
628 (cDNA) was amplified using the KOD One PCR Master Mix -Blue- (TOYOBO, Cat# KMM-201).  
629 The obtained fragment was digested with XbaI (NEB, Cat# R0145) and NotI (NEB, Cat# R0189) and  
630 ligated with PB514B-2, which was also digested with XbaI and NotI, using the TAKARA Ligation kit  
631 ver.2.1 (TAKARA Bio, Cat# 6022).

632

### 633 **Isolation of TS mutants**

634 To obtain TS mutants, a previously reported protocol for the induction of mutations in MHV was  
635 followed (Deng et al., 2019). Briefly, the clinical isolate strain B-1 was used to infect confluent Vero  
636 cells in six-well plates for 1 h at 37°C. A fresh medium containing 5-fluorouracil (100  $\mu$ g/mL,

637 FUJIFILM Wako, Cat# 068-01401) was added. After a one-day incubation period at 32°C, the  
638 supernatants were collected and stocked as “mutated virus”. These viruses were passaged three times  
639 in Vero cells at 32°C, and viral clones were obtained by plaque isolation. The collected plaques were  
640 suspended in 100 µL DMEM and an aliquot of 2-50 µL of this suspension was used to infect Vero  
641 cells at 32°C. To confirm temperature sensitivity, we observed the development of CPE at 37 or  
642 32°C.

643

#### 644 **Construction of recombinant viruses using circular polymerase extension reaction (CPER)**

645 Viruses bearing TS mutations were constructed using circular polymerase extension reaction (CPER)  
646 (Torii et al., 2021), with minor modifications. We cloned the fragmented B-1 viral genome into  
647 plasmids. TS mutations of interest were introduced into these plasmids using inverse PCR. We then  
648 assembled these fragments by CPER using PrimeSTAR GXL DNA polymerase (Takara Bio, Cat#  
649 R050A). The assembled cDNA was transfected into BHK-hACE2 cells using Lipofectamine LTX  
650 Reagent with PLUS™ Reagent (Invitrogen, Cat# 15338100). Seven days after transfection,  
651 supernatants were collected. The supernatant was used to inoculate VeroE6-TMPRSS2 and incubated  
652 for four days. After observing CPE, the supernatant was collected and used to inoculate Vero cells to  
653 harvest the desired SARS-CoV2 viruses. To obtain TS-recombinant viruses, we performed a  
654 construction experiment at 32-34°C.

655

#### 656 **Titration assay**

657 Viral titration was determined using the 50% tissue culture infectious dose (TCID<sub>50</sub>) or plaque  
658 formation units (PFU). Briefly, samples were serially diluted in DMEM supplemented with 2% FBS  
659 and antibiotics. Fifty microliters of diluted samples were used to infect confluent Vero cells in 96-well  
660 plates and incubated at 37°C (wild-type strain) or 32°C (TS strain) for six days. Infected cells were  
661 fixed with 10% formalin and stained with crystal violet. After staining, the TCID<sub>50</sub> was calculated  
662 using the Behrens-Karber method. For the plaque formation assay, diluted samples were used to infect  
663 confluent Vero cells in 6-well plates for 1 h at 32 or 37°C. Cells were then washed with D-PBS. After  
664 washing, a fresh medium containing 1% SeaPlaque Agarose (Lonza, Cat# 50100) was layered and  
665 incubated at 32 or 37°C until plaque formation. Cells were fixed in 10% formalin and stained with  
666 crystal violet. Visible plaques were counted to calculate the PFU.

667

#### 668 **NGS analysis**

669 Vero cells were infected with wild-type or TS SARS-CoV-2 and incubated at 37 or 32°C, respectively.  
670 After three days, supernatants were collected, and RNA was extracted using a QIAamp Viral RNA  
671 Mini Kit (Qiagen, Cat# 52904) according to the manufacturer's protocol. Viral RNA was processed  
672 and analyzed at the Genome Information Research Center of Osaka University using NovaSeq6000

673 (Illumina). Wuhan strain (NC045512) was used as the reference sequence.

674

#### 675 **Determination of viral growth dynamics**

676 One million Vero cells per well were cultured in six-well plates and incubated at 37°C overnight.  
677 SARS-CoV-2 strain suspensions ( $1 \times 10^4$  TCID<sub>50</sub>) were used to inoculate the cells (MOI = 0.01), which  
678 were then incubated at 32, 34, or 37°C for five days. The supernatants were collected and stored at  
679 -80°C daily. Viral titration of the supernatants was performed using TCID<sub>50</sub>/mL, as described above.  
680 Each experiment was performed in triplicate.

681

#### 682 **Neutralization assay**

683 Serum samples were inactivated by incubation at 56°C for 30 min and serially diluted with DMEM  
684 supplemented with 2% FBS. Serially diluted serum was mixed with 100 TCID<sub>50</sub> of SARS-CoV-2 B-  
685 1, Delta, Gamma, or Omicron strains and incubated at 37°C for 1 h. After incubation, the samples  
686 were used to inoculate confluent Vero cells in 96-well plates and were incubated at 37°C for seven  
687 days. Cells were fixed in formalin and stained with crystal violet. Neutralizing titers were determined  
688 as the inverse of the maximum dilution that prevented viral proliferation.

689 For the neutralization assay of nasal wash specimens, we performed an assay using the pseudotyped  
690 VSV virus. Briefly, the VSVΔG/Luc-encoding SARS-CoV-2 S-expressing pseudovirus was mixed  
691 and co-incubated with the same volume of nasal wash and incubated for one hour. Mixtures were  
692 added to Vero cells and the cells were lysed using lysis buffer (Promega, Cat# E153A) after incubation  
693 for 24 h. Luciferase activity was measured using a ONE-Glo™ EX Luciferase Assay System (Promega,  
694 Cat# E8130).

695

#### 696 **Generation and characterization of revertants**

697 To obtain revertants, TS strains were used to infect confluent Vero cells at 37, 38, and 39°C (MOI =  
698 1). Viruses from the CPE-positive wells were further propagated in Vero cells at 37 or 38°C to obtain  
699 the corresponding viral stocks. To identify any mutations around the nucleotide of interest in the  
700 revertants, viral genomic RNA was extracted using TriReagent (Molecular Research Center, Cat#  
701 TR118) or a QIAamp viral RNA mini kit (Qiagen, Cat# 52904), according to the manufacturer's  
702 protocols, and subsequently subjected to cDNA synthesis using the SuperScript™ III First-Strand  
703 Synthesis System for RT-PCR (Invitrogen, Cat# 11904018). The genomic regions surrounding each  
704 mutation of interest in Table 1 were amplified by PCR using specific primers. The PCR products were  
705 sequenced and compared with those of the corresponding parental TS strains.

706

#### 707 ***In vitro* and *in vivo* evaluation of the “reversion-to-virulence” risk of each mutant**

708 To estimate the risk of each TS strain reverting to the virulent phenotype *in vitro*, each TS virus was

709 used to infect confluent Vero cells ( $5 \times 10^3$  TCID<sub>50</sub>/well) in 96-well plates, which were maintained for  
710 one or two days at 32°C. Subsequently, they were passaged independently in new confluent Vero cells  
711 in 96-well plates and maintained for additional three days at 39°C. After incubation, the number of  
712 CPE-positive wells was counted. Eventually, we confirmed the viral sequence, as described above. To  
713 confirm the risk of rTS-all reverting to the virulent phenotype *in vivo*, rTS-all and L50-33 viruses were  
714 used to infect Syrian hamsters (5 weeks, male, n = 3) at  $1.8 \times 10^5$  TCID<sub>50</sub>/100 µL/dose. Nasal wash  
715 specimens were collected with 500 µL of D-PBS three dpi. The viral titer in each sample was  
716 calculated as described above. To determine the genomic sequence of the virus in each sample, viral  
717 RNA was extracted and sanger sequenced as described above.

718

### 719 **QUANTIFICATION AND STATISTICAL ANALYSIS**

720 Each data point is expressed as the mean ± SD or median ± 95% CI. To analyze the viral titer in the  
721 nasal wash or lung samples, statistical analyses were performed using one-way ANOVA. For the  
722 analysis of the neutralization titer, the Kruskal-Wallis test was used to calculate statistical significance.  
723 For the analysis of the viral growth kinetics and *in vivo* weight change, two-way ANOVA was  
724 performed. For samples below the LOD, the assay's LOD was used to calculate the mean. All analyses  
725 were performed using the GraphPad Prism software (n.s.: not significant, \*p < 0.05, \*\*p < 0.01, \*\*\*p  
726 < 0.001, and \*\*\*\*p < 0.0001).

727

### 728 **REFERENCES**

- 729 Baum, A., Fulton, B.O., Wloga, E., Copin, R., Pascal, K.E., Russo, V., Giordano, S., Lanza, K., Negron,  
730 N., Ni, M., et al. (2020). Antibody cocktail to SARS-CoV-2 spike protein prevents rapid mutational  
731 escape seen with individual antibodies. *Science* 369, 1014-1018. doi:10.1126/science.abd0831.
- 732 CDC. Centers for Disease Control and Prevention. COVID Data Tracker. [https://covid.cdc.gov/covid-](https://covid.cdc.gov/covid-data-tracker/)  
733 [data-tracker/](https://covid.cdc.gov/covid-data-tracker/).
- 734 Chen, Y., Cai, H., Pan, J.a., Xiang, N., Tien, P., Ahola, T., and Guo, D. (2009). Functional screen reveals  
735 SARS coronavirus nonstructural protein nsp14 as a novel cap N7 methyltransferase. *Proc. Natl. Acad.*  
736 *Sci. U S A* 106, 3484-3489. doi:10.1073/pnas.0808790106.
- 737 Chen, Y., Su, C., Ke, M., Jin, X., Xu, L., Zhang, Z., Wu, A., Sun, Y., Yang, Z., Tien, P., et al. (2011).  
738 Biochemical and Structural Insights into the Mechanisms of SARS Coronavirus RNA Ribose 2' -O-  
739 Methylation by nsp16/nsp10 Protein Complex. *PLOS Pathog.* 7, e1002294.  
740 10.1371/journal.ppat.1002294.
- 741 Cox, A., and Dewhurst, S. (2015). A Single Mutation at PB1 Residue 319 Dramatically Increases the  
742 Safety of PR8 Live Attenuated Influenza Vaccine in a Murine Model without Compromising Vaccine  
743 Efficacy. *J. Virol.* 90, 2702-2705. 10.1128/JVI.02723-15.
- 744 Decroly, E., Debarnot, C., Ferron, F., Bouvet, M., Coutard, B., Imbert, I., Gluais, L., Papageorgiou, N.,

- 745 Sharff, A., Bricogne, G., et al. (2011). Crystal structure and functional analysis of the SARS-coronavirus  
746 RNA cap 2'-O-methyltransferase nsp10/nsp16 complex. *PLoS Pathog.* 7, e1002059.  
747 10.1371/journal.ppat.1002059.
- 748 Decroly, E., Imbert, I., Coutard, B., Bouvet, M., Selisko, B., Alvarez, K., Gorbalenya, A.E., Snijder, E.J.,  
749 and Canard, B. (2008). Coronavirus nonstructural protein 16 is a cap-0 binding enzyme possessing  
750 (nucleoside-2'O)-methyltransferase activity. *J. Virol.* 82, 8071-8084. 10.1128/JVI.00407-08.
- 751 Deng, X., Mettelman, R.C., O'Brien, A., Thompson, J.A., O'Brien, T.E., and Baker, S.C. (2019). Analysis  
752 of Coronavirus Temperature-Sensitive Mutants Reveals an Interplay between the Macrodomein and  
753 Papain-Like Protease Impacting Replication and Pathogenesis. *J. Virol.* 93. 10.1128/JVI.02140-18.
- 754 Edara, V.V., Norwood, C., Floyd, K., Lai, L., Davis-Gardner, M.E., Hudson, W.H., Mantus, G., Nyhoff,  
755 L.E., Adelman, M.W., Fineman, R., et al. (2021). Infection- and vaccine-induced antibody binding and  
756 neutralization of the B.1.351 SARS-CoV-2 variant. *Cell Host Microbe* 29, 516-521.e513.  
757 <https://doi.org/10.1016/j.chom.2021.03.009>.
- 758 Folegatti, P.M., Ewer, K.J., Aley, P.K., Angus, B., Becker, S., Belij-Rammerstorfer, S., Bellamy, D., Bibi,  
759 S., Bittaye, M., Clutterbuck, E.A., et al. (2020). Safety and immunogenicity of the ChAdOx1 nCoV-19  
760 vaccine against SARS-CoV-2: a preliminary report of a phase 1/2, single-blind, randomised controlled  
761 trial. *Lancet* 396, 467-478. 10.1016/S0140-6736(20)31604-4.
- 762 Giacomelli, A., Pezzati, L., Conti, F., Bernacchia, D., Siano, M., Oreni, L., Rusconi, S., Gervasoni, C.,  
763 Ridolfo, A.L., Rizzardini, G., et al. (2020). Self-reported Olfactory and Taste Disorders in Patients With  
764 Severe Acute Respiratory Coronavirus 2 Infection: A Cross-sectional Study. *Clin. Infect. Dis.* 71, 889-  
765 890. 10.1093/cid/ciaa330.
- 766 Grifoni, A., Weiskopf, D., Ramirez, S.I., Mateus, J., Dan, J.M., Moderbacher, C.R., Rawlings, S.A.,  
767 Sutherland, A., Premkumar, L., Jadi, R.S., et al. (2020). Targets of T Cell Responses to SARS-CoV-2  
768 Coronavirus in Humans with COVID-19 Disease and Unexposed Individuals. *Cell* 181, 1489-  
769 1501.e1415. <https://doi.org/10.1016/j.cell.2020.05.015>.
- 770 Imai, M., Iwatsuki-Horimoto, K., Hatta, M., Loeber, S., Halfmann, P.J., Nakajima, N., Watanabe, T., Ujie,  
771 M., Takahashi, K., Ito, M., et al. (2020). Syrian hamsters as a small animal model for SARS-CoV-2  
772 infection and countermeasure development. *Proc. Natl. Acad. Sci. U S A* 117, 16587-16595.  
773 10.1073/pnas.2009799117.
- 774 Jackson, L.A., Anderson, E.J., Roupheal, N.G., Roberts, P.C., Makhene, M., Coler, R.N., McCullough,  
775 M.P., Chappell, J.D., Denison, M.R., Stevens, L.J., et al. (2020). An mRNA Vaccine against SARS-CoV-2  
776 — Preliminary Report. *N. Engl. J. Med.* 383, 1920-1931. 10.1056/NEJMoa2022483.
- 777 Jumper, J., Evans, R., Pritzel, A., Green, T., Figurnov, M., Ronneberger, O., Tunyasuvunakool, K., Bates,  
778 R., Židek, A., Potapenko, A., et al. (2021). Highly accurate protein structure prediction with AlphaFold.  
779 *Nature* 596, 583-589. 10.1038/s41586-021-03819-2.
- 780 Kew, O.M., Sutter, R.W., Gourville, E.M.d., Dowdle, W.R., and Pallansch, M.A. (2005). VACCINE-

- 781 DERIVED POLIOVIRUSES AND THE ENDGAME STRATEGY FOR GLOBAL POLIO  
782 ERADICATION. *Annu. Rev. Microbiol.* 59, 587-635. 10.1146/annurev.micro.58.030603.123625.
- 783 Khan, M., Yoo, S.-J., Clijsters, M., Backaert, W., Vanstapel, A., Speleman, K., Lietaer, C., Choi, S.,  
784 Hether, T.D., Marcelis, L., et al. (2021). Visualizing in deceased COVID-19 patients how SARS-CoV-2  
785 attacks the respiratory and olfactory mucosae but spares the olfactory bulb. *Cell* 184, 5932-5949.e5915.  
786 <https://doi.org/10.1016/j.cell.2021.10.027>.
- 787 Komase, K., Nakayama, T., Iijima, M., Miki, K., Kawanishi, R., and Uejima, H. (2006). The  
788 phosphoprotein of attenuated measles AIK-C vaccine strain contributes to its temperature-sensitive  
789 phenotype. *Vaccine* 24, 826-834. 10.1016/j.vaccine.2005.06.036.
- 790 Krafcikova, P., Silhan, J., Nencka, R., and Boura, E. (2020). Structural analysis of the SARS-CoV-2  
791 methyltransferase complex involved in RNA cap creation bound to sinefungin. *Nat. Commun.* 11, 3717.  
792 10.1038/s41467-020-17495-9.
- 793 Maassab, H.F., and Bryant, M.L. (1999). The development of live attenuated cold-adapted influenza virus  
794 vaccine for humans. *Rev. Med. Virol.* 9, 237-244. 10.1002/(sici)1099-1654(199910/12)9:4<237::aid-  
795 rmv252>3.0.co;2-g.
- 796 Makino, S., Sasaki, K., Nazari, F., Nakagawa, M., and Nakamura, N. (1970). Cultivation of measles virus  
797 in sheep kidney cells. *Jpn. J. Microbiol.* 14, 501-504.
- 798 Minskaia, E., Hertzog, T., Gorbalenya Alexander, E., Campanacci, V., Cambillau, C., Canard, B., and  
799 Ziebuhr, J. (2006). Discovery of an RNA virus 3' → 5' exoribonuclease that is critically involved in  
800 coronavirus RNA synthesis. *Proc. Natl. Acad. Sci. U S A* 103, 5108-5113. 10.1073/pnas.0508200103.
- 801 Murphy, B.R., and Coelingh, K. (2002). Principles underlying the development and use of live attenuated  
802 cold-adapted influenza A and B virus vaccines. *Viral Immunol.* 15, 295-323.  
803 10.1089/08828240260066242.
- 804 Ogando, N.S., Zevenhoven-Dobbe, J.C., van der Meer, Y., Bredenbeek, P.J., Posthuma, C.C., and Snijder,  
805 E.J. (2020). The Enzymatic Activity of the nsp14 Exoribonuclease Is Critical for Replication of MERS-  
806 CoV and SARS-CoV-2. *J. Virol.* 94. 10.1128/JVI.01246-20.
- 807 Okamoto, K., Ami, Y., Suzaki, Y., Otsuki, N., Sakata, M., Takeda, M., and Mori, Y. (2016). Analysis of  
808 the temperature sensitivity of Japanese rubella vaccine strain TO-336.vac and its effect on  
809 immunogenicity in the guinea pig. *Virology* 491, 89-95. 10.1016/j.virol.2016.01.027.
- 810 [ourworldindata.org](https://ourworldindata.org). Coronavirus Pandemic (COVID-19). <https://ourworldindata.org/coronavirus>.
- 811 Pape, K.A., Dileepan, T., Kabage, A.J., Kozysa, D., Batres, R., Evert, C., Matson, M., Lopez, S., Krueger,  
812 P.D., Graiziger, C., et al. (2021). High-affinity memory B cells induced by SARS-CoV-2 infection  
813 produce more plasmablasts and atypical memory B cells than those primed by mRNA vaccines. *Cell Rep.*  
814 37, 109823. <https://doi.org/10.1016/j.celrep.2021.109823>.
- 815 Parks, C.L., Lerch, R.A., Walpita, P., Wang, H.P., Sidhu, M.S., and Udem, S.A. (2001). Comparison of  
816 predicted amino acid sequences of measles virus strains in the Edmonston vaccine lineage. *J. Virol.* 75,

- 817 910-920. 10.1128/JVI.75.2.910-920.2001.
- 818 Piano Mortari, E., Russo, C., Vinci, M.R., Terreri, S., Fernandez Salinas, A., Piccioni, L., Alteri, C.,  
819 Colagrossi, L., Coltella, L., Ranno, S., et al. (2021). Highly Specific Memory B Cells Generation after the  
820 2nd Dose of BNT162b2 Vaccine Compensate for the Decline of Serum Antibodies and Absence of  
821 Mucosal IgA. *Cells* 10, 2541.
- 822 Sahin, U., Muik, A., Derhovanessian, E., Vogler, I., Kranz, L.M., Vormehr, M., Baum, A., Pascal, K.,  
823 Quandt, J., Maurus, D., et al. (2021). Publisher Correction: COVID-19 vaccine BNT162b1 elicits human  
824 antibody and TH1 T cell responses. *Nature* 590, E17-E17. 10.1038/s41586-020-03102-w.
- 825 Sasaki, K. (1974). Studies on the modification of the live AIK measles vaccine. I. Adaptation of the  
826 further attenuated AIK measles virus (the strain AIK-L33) to chick embryo cells. *Kitasato Arch. Exp.*  
827 *Med.* 47, 1-12.
- 828 Sekine, T., Perez-Potti, A., Rivera-Ballesteros, O., Strålin, K., Gorin, J.-B., Olsson, A., Llewellyn-Lacey,  
829 S., Kamal, H., Bogdanovic, G., Muschiol, S., et al. (2020). Robust T Cell Immunity in Convalescent  
830 Individuals with Asymptomatic or Mild COVID-19. *Cell* 183, 158-168.e114.  
831 <https://doi.org/10.1016/j.cell.2020.08.017>.
- 832 Seo, S.H., and Jang, Y. (2020). Cold-Adapted Live Attenuated SARS-Cov-2 Vaccine Completely Protects  
833 Human ACE2 Transgenic Mice from SARS-Cov-2 Infection. *Vaccines (Basel)* 8.  
834 10.3390/vaccines8040584.
- 835 Shah, V.K., Fimal, P., Alam, A., Ganguly, D., and Chattopadhyay, S. (2020). Overview of Immune  
836 Response During SARS-CoV-2 Infection: Lessons From the Past. *Front. Immunol.* 11.  
837 10.3389/fimmu.2020.01949.
- 838 Shishido, A., and Ohtawara, M. (1976). Development of attenuated rubella virus vaccines in Japan. *Jpn. J.*  
839 *Med. Sci. Biol.* 29, 227-253. 10.7883/yoken1952.29.227.
- 840 Sia, S.F., Yan, L.M., Chin, A.W.H., Fung, K., Choy, K.T., Wong, A.Y.L., Kaewpreedee, P., Perera, R.,  
841 Poon, L.L.M., Nicholls, J.M., et al. (2020). Pathogenesis and transmission of SARS-CoV-2 in golden  
842 hamsters. *Nature* 583, 834-838. 10.1038/s41586-020-2342-5.
- 843 Sterlin, D., Mathian, A., Miyara, M., Mohr, A., Anna, F., Claër, L., Quentric, P., Fadlallah, J., Devilliers,  
844 H., Ghillani, P., et al. (2021). IgA dominates the early neutralizing antibody response to SARS-CoV-2.  
845 *Sci. Transl. Med.* 13, eabd2223. doi:10.1126/scitranslmed.abd2223.
- 846 Takahashi, M., Otsuka, T., Okuno, Y., Asano, Y., and Yazaki, T. (1974). Live vaccine used to prevent the  
847 spread of varicella in children in hospital. *Lancet* 2, 1288-1290. 10.1016/s0140-6736(74)90144-5.
- 848 Tani, H., Shiokawa, M., Kaname, Y., Kambara, H., Mori, Y., Abe, T., Moriishi, K., and Matsuura, Y.  
849 (2010). Involvement of Ceramide in the Propagation of Japanese Encephalitis Virus. *J. Virol.* 84, 2798-  
850 2807. doi:10.1128/JVI.02499-09.
- 851 Torii, S., Ono, C., Suzuki, R., Morioka, Y., Anzai, I., Fauzyah, Y., Maeda, Y., Kamitani, W., Fukuhara, T.,  
852 and Matsuura, Y. (2021). Establishment of a reverse genetics system for SARS-CoV-2 using circular

853 polymerase extension reaction. *Cell Rep.* 35. 10.1016/j.celrep.2021.109014.

854 Trimpert, J., Dietert, K., Firsching, T.C., Ebert, N., Thi Nhu Thao, T., Vladimirova, D., Kaufer, S.,  
855 Labroussaa, F., Abdelgawad, A., Conradie, A., et al. (2021). Development of safe and highly protective  
856 live-attenuated SARS-CoV-2 vaccine candidates by genome recoding. *Cell Rep.* 36, 109493.  
857 10.1016/j.celrep.2021.109493.

858 Urata, S., Maruyama, J., Kishimoto-Urata, M., Sattler, R.A., Cook, R., Lin, N., Yamasoba, T., Makishima,  
859 T., and Paessler, S. (2021). Regeneration Profiles of Olfactory Epithelium after SARS-CoV-2 Infection in  
860 Golden Syrian Hamsters. *ACS Chem. Neurosci.* 10.1021/acchemneuro.0c00649.

861 Wang, Y., Yang, C., Song, Y., Coleman, J.R., Stawowczyk, M., Tafrova, J., Tasker, S., Boltz, D., Baker,  
862 R., Garcia, L., et al. (2021). Scalable live-attenuated SARS-CoV-2 vaccine candidate demonstrates  
863 preclinical safety and efficacy. *Proc. Natl. Acad. Sci. U S A* 118. 10.1073/pnas.2102775118.

864 Wibmer, C.K., Ayres, F., Hermanus, T., Madzivhandila, M., Kgagudi, P., Oosthuysen, B., Lambson, B.E.,  
865 de Oliveira, T., Vermeulen, M., van der Berg, K., et al. (2021). SARS-CoV-2 501Y.V2 escapes  
866 neutralization by South African COVID-19 donor plasma. *Nat. Med.* 27, 622-625. 10.1038/s41591-021-  
867 01285-x.

868 Ye, Z.W., Ong, C.P., Tang, K., Fan, Y., Luo, C., Zhou, R., Luo, P., Cheng, Y., Gray, V.S., Wang, P., et al.  
869 (2022). Intranasal administration of a single dose of a candidate live attenuated vaccine derived from an  
870 NSP16-deficient SARS-CoV-2 strain confers sterilizing immunity in animals. *Cell Mol Immunol* 19, 588-  
871 601. 10.1038/s41423-022-00855-4.

872 Zhou, D., Chan, J.F.-W., Zhou, B., Zhou, R., Li, S., Shan, S., Liu, L., Zhang, A.J., Chen, S.J., Chan, C.C.-  
873 S., et al. (2021). Robust SARS-CoV-2 infection in nasal turbinates after treatment with systemic  
874 neutralizing antibodies. *Cell Host Microbe* 29, 551-563.e555.  
875 <https://doi.org/10.1016/j.chom.2021.02.019>.

876 Zimmerman, L.A., Reef, S.E., and Orenstein, W.A. (2018). Rubella Vaccine-A Tale of Appropriate  
877 Caution and Remarkable Success. *JAMA Pediatr.* 172, 95-96. 10.1001/jamapediatrics.2017.4178.  
878  
879

Table 1. Genetic mutation and amino acid substitution in the TS strains

Strain	Genetic mutation	Protein	Amino acid substitution
A50-18	G18782T	nsp14	G248V
	G19285A		G416S
	C19550T		A504V
	C24198T	Spike	A879V
	T26327C	Envelope	L28P
	C28278T	Nucleocapsid	S2F
H50-11 <sup>a</sup>	T3930C	nsp3	V404A
	G8213A		D1832N
	G20857A	nsp16	V67I
	C23778A	Spike	T739K
L50-33 <sup>a</sup>	C4052T	nsp3	L445F
	A8094G		K1792R
L50-40 <sup>a</sup>	C4052T	nsp3	L445F
	A8094G		K1792R
	T21723G	Spike	L54W

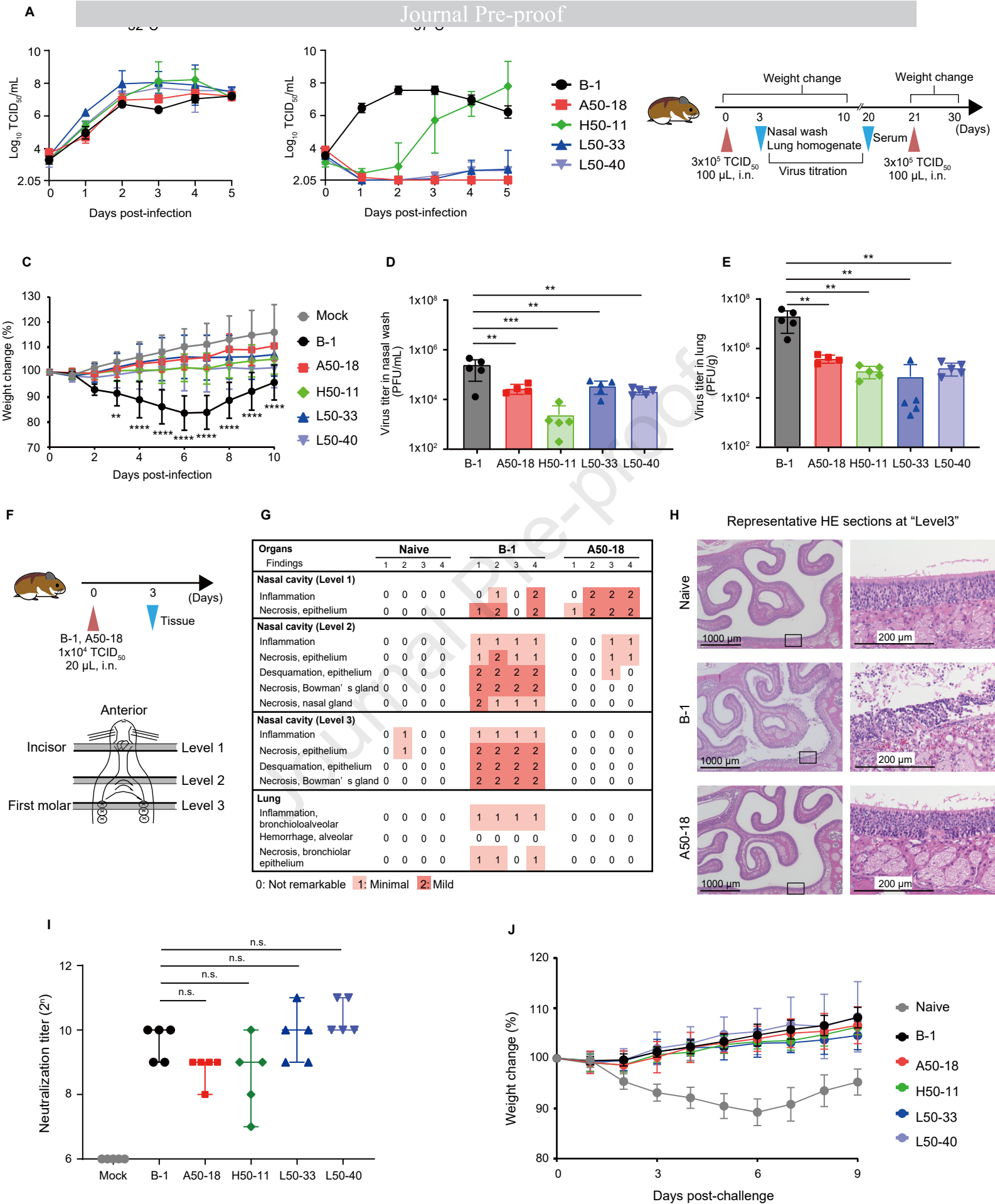
<sup>a</sup> H50-11, L50-33, L50-40 strains had a common deletion in *orf7a-orf8* (27549-28251).

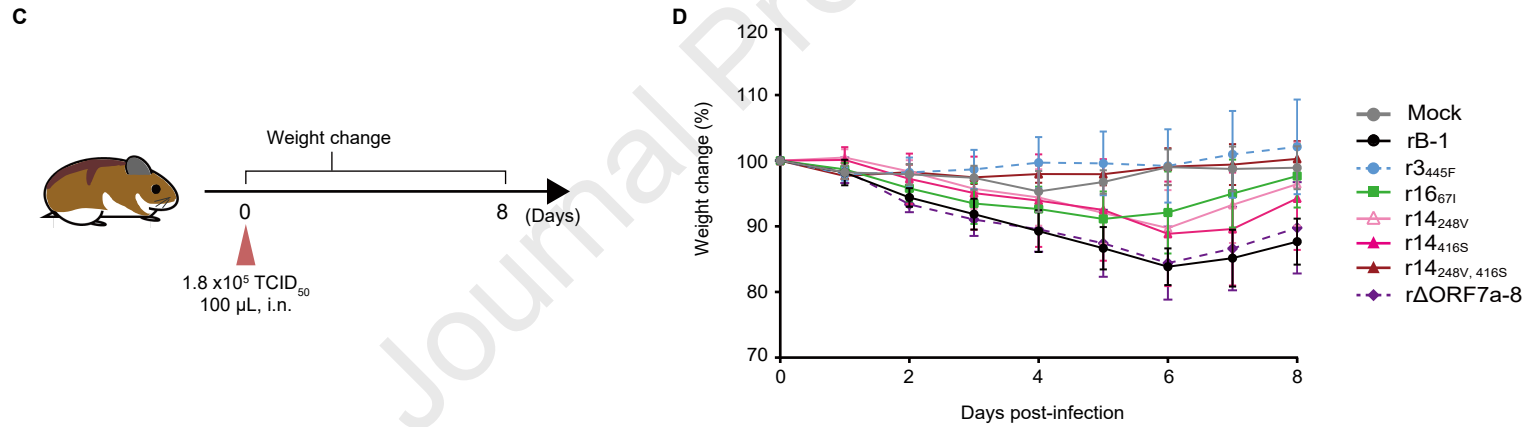
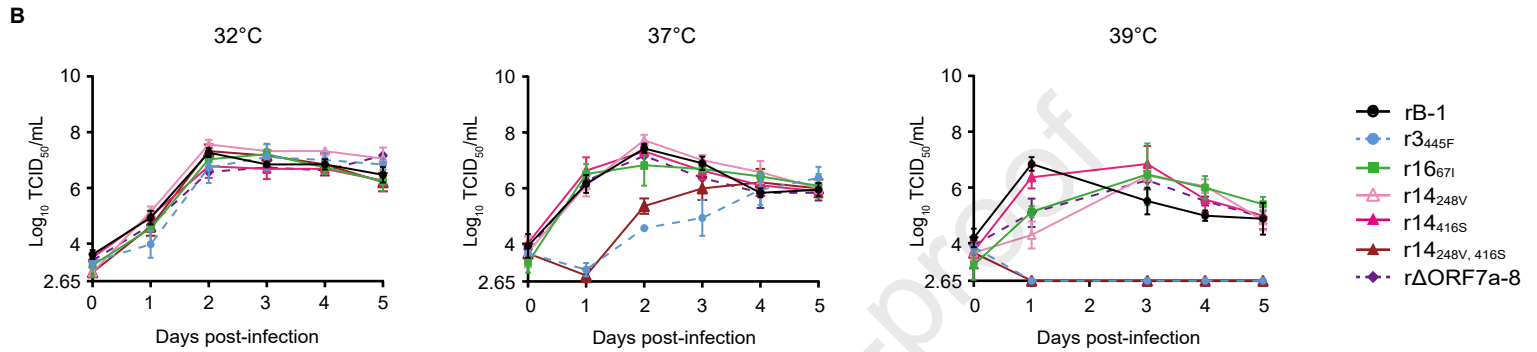
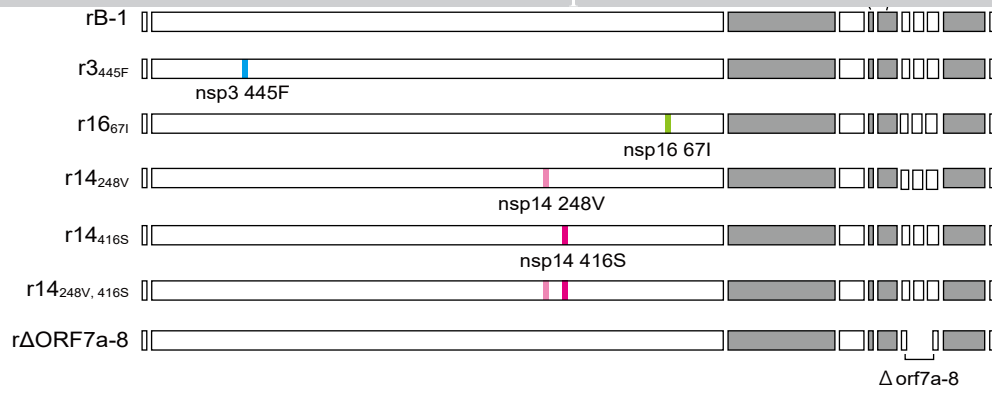
Table2. Amino acid substitutions in the revertants

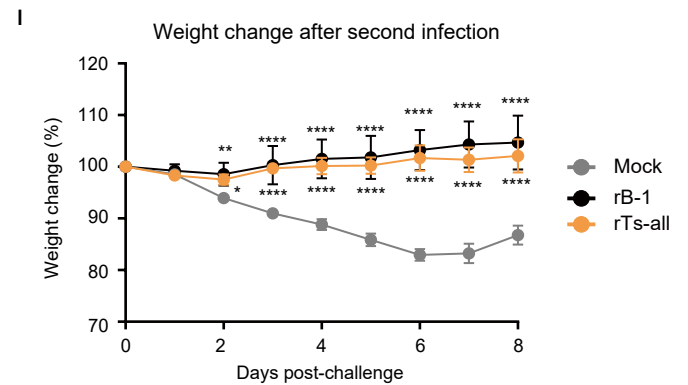
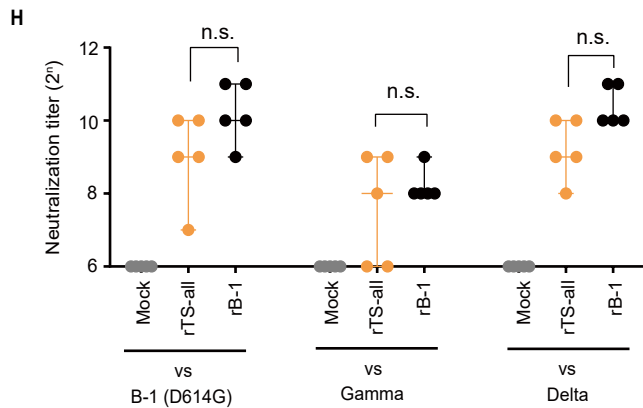
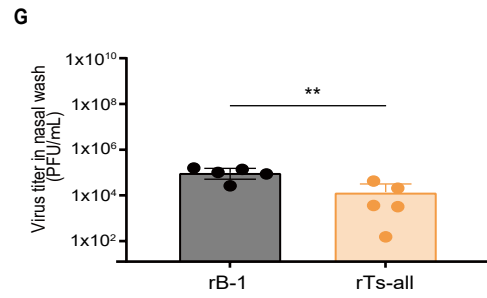
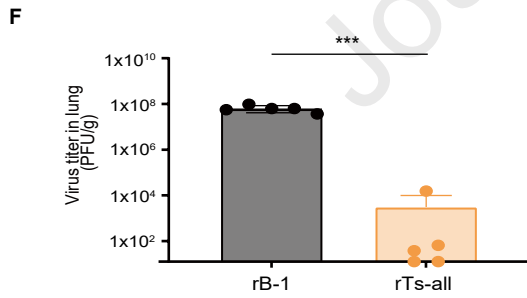
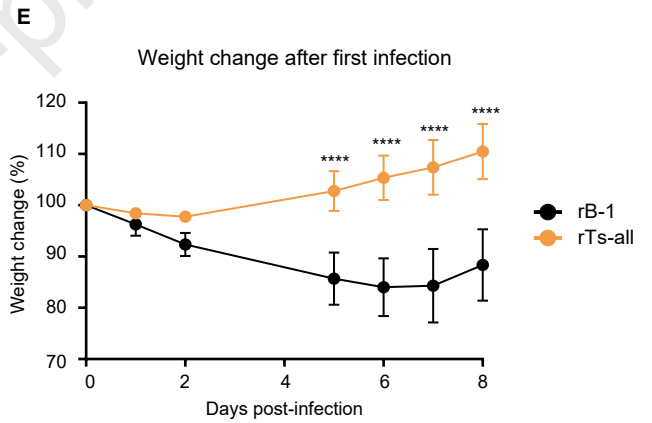
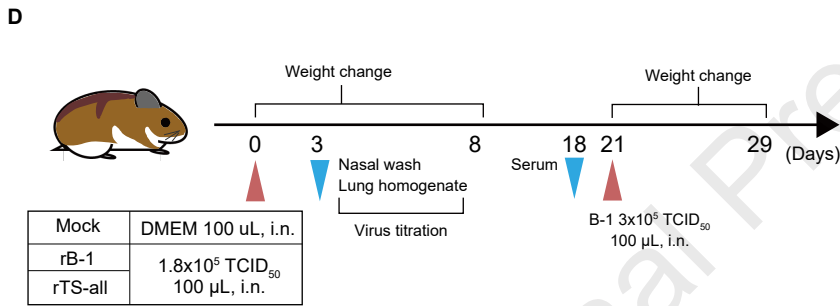
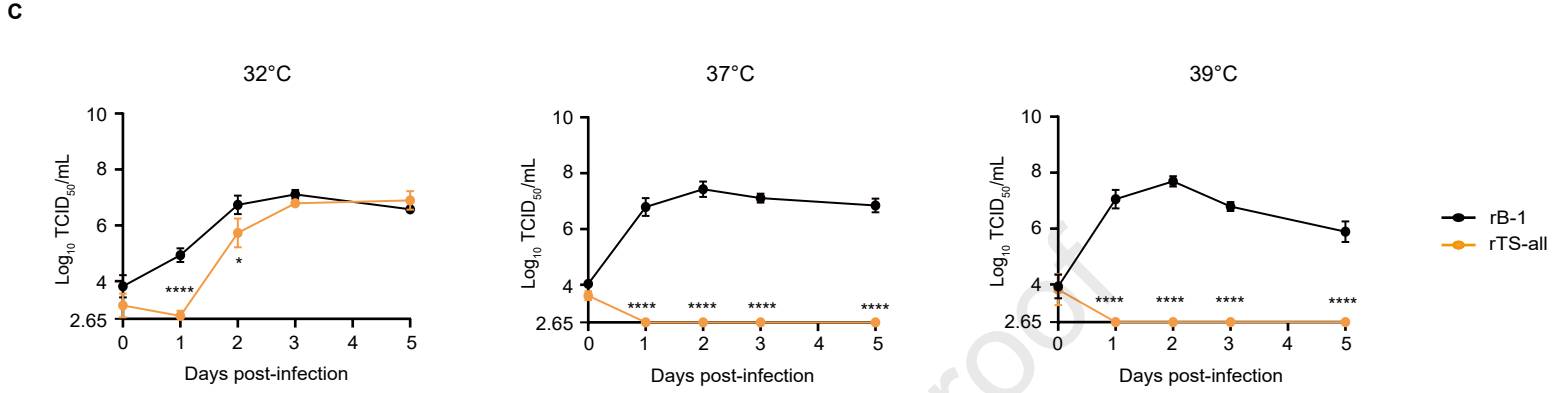
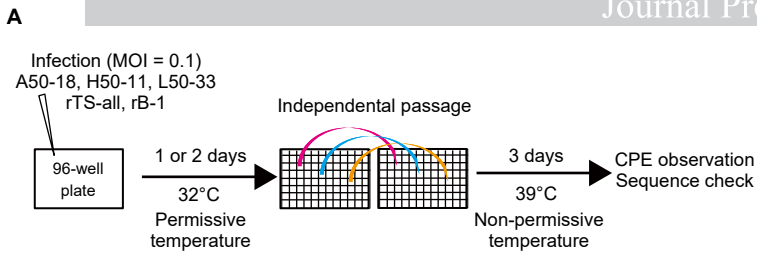
37°C					38°C				39°C			
Parent TS strain	Revertants <sup>a</sup>	Amino acid substitution	Codon change	Rate <sup>b</sup>	Revertants <sup>a</sup>	Amino acid substitution	Codon change	Rate <sup>b</sup>	Revertants <sup>a</sup>	Amino acid substitution	Codon change	Rate <sup>b</sup>
<b>A50-18</b>	19/230	nsp14 248G	GTG>GGT	6/19	5/223	nsp14 416G	AGT>GGT	5/5	0/230	-	-	-
		nsp14 416G	AGT>GGT	13/19								
<b>H50-11</b>	2/230	nsp16 67V	ATT>GTT	2/2	1/240	nsp16 67V	ATT>GTT	1/1	0/237	-	-	-
<b>L50-33</b>	34/230		TTT>CTT	4/34	39/228		TTT>CTT	2/39	13/230		TTT>CTT	2/13
		nsp3 445L	TTT>TTG	17/34		nsp3 445L	TTT>TTG	22/39		nsp3 445L	TTT>TTG	6/13
			TTT>TTA	1/34			TTT>TTA	3/39			TTT>TTA	1/13
		nsp3 445C	TTT>TGT	8/34		nsp3 445C	TTT>TGT	7/39		nsp3 445C	TTT>TGT	2/13
		nsp3 445V	TTT>GTT	3/34		nsp3 445V	TTT>GTT	3/39		nsp3 445V	TTT>GTT	2/13
		nsp3 445I	TTT>ATT	1/34		nsp3 445I	TTT>ATT	2/39				
<b>L50-40</b>	17/230	nsp3 445L	TTT>CTT	2/17	14/228	nsp3 445L	TTT>CTT	2/14	4/216	nsp3 445L	TTT>CTT	2/4
			TTT>TTG	9/17			TTT>TTG	9/14			TTT>TTG	1/4
		nsp3 445C	TTT>TGT	6/17		nsp3 445C	TTT>TGT	3/14		nsp3 445C	TTT>TGT	1/4

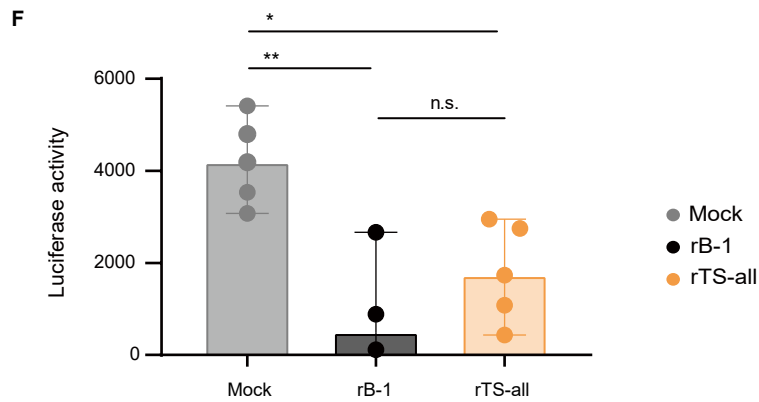
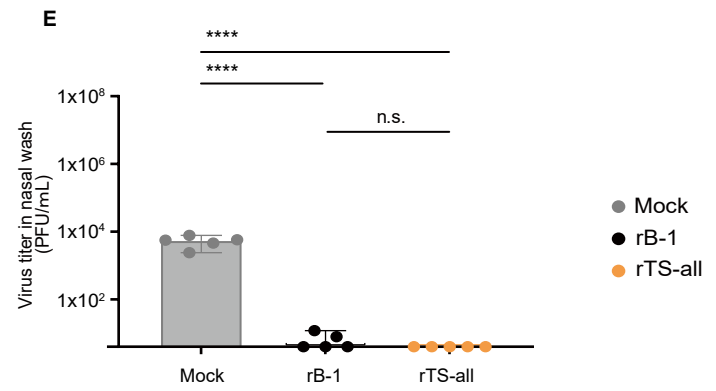
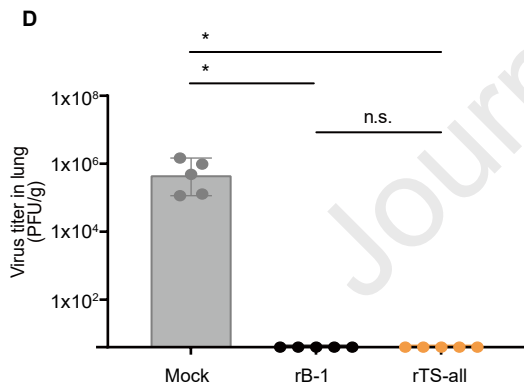
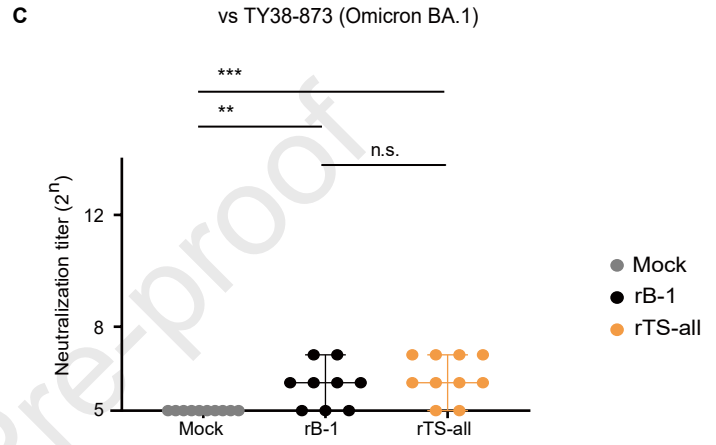
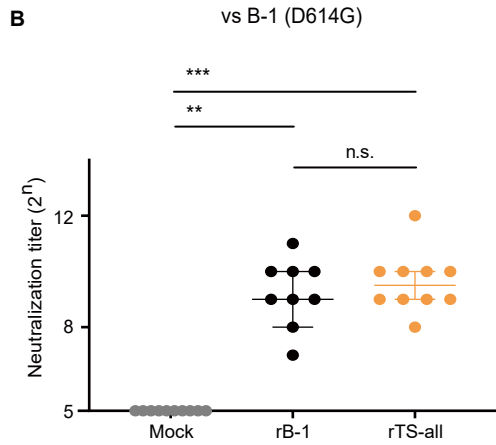
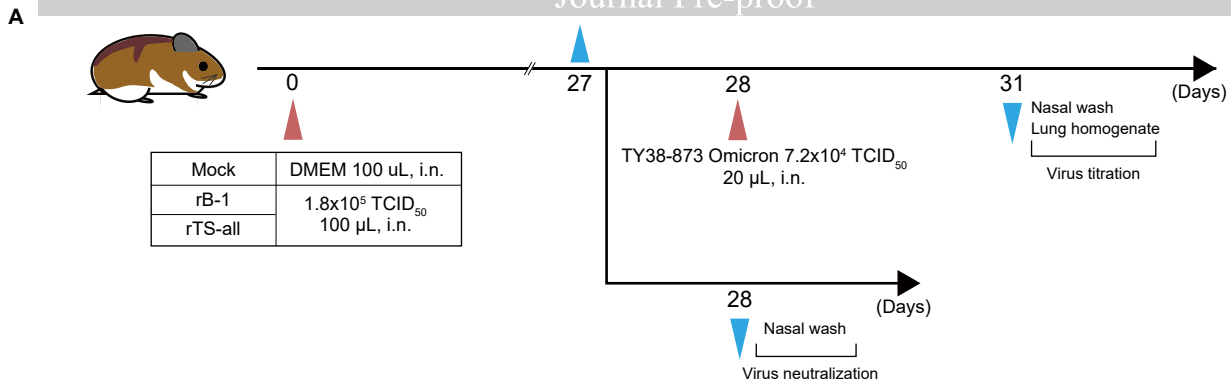
<sup>a</sup>: Number of wells with revertants/Total.

<sup>b</sup>: Rate of wells containing viruses with the specified codon changes.











- Temperature-sensitive CoV-2 with mutations in *nsp3*, *nsp14* and *nsp16* were isolated.
- Combination of these mutations led to reduced risk of virulent reversion.
- Engineered viral strain showed strong immunogenicity *in vivo*.
- A live-attenuated vaccine platform with exchangeable spike protein was established.

Journal Pre-proof

**STAR★Methods****KEY RESOURCE TABLE**

REAGENT or RESOURCE	SOURCE	IDENTIFIER
<b>Bacterial and virus strains</b>		
SARS-CoV-2: pre-alpha type, D614G, B-1 strain	This paper	NCBI: LC603286
SARS-CoV-2: gamma variant, TY7-501 strain	National Institute of Infectious Diseases	GISAID ID : EPI_ISL_833366
SARS-CoV-2: delta variant, BK325 strain	Research Foundation for Microbial Diseases of Osaka University	N/A
SARS-CoV-2: omicron variant, TY38-873 strain	National Institute of Infectious Diseases	GISAID ID : EPI_ISL_7418017
<b>Chemicals, peptides, and recombinant proteins</b>		
5-fluorouracil	FUJIFILM Wako	Cat# 068-01401
KOD One PCR Master Mix -Blue-	TOYOBO	Cat# KMM-201
PrimeSTAR GXL DNA polymerase	TaKaRa Bio	Cat# R050A
Lipofectamin LTX Reagent with PLUS™ Reagent	Invitrogen	Cat# 15338100
SeaPlaque Agarose	LONZA	Cat# 50100
TriReagent	Molecular Research Center	Cat# TR118
Luciferase Cell Culture Lysis 5X Reagent	Promega	Cat# E153A
Hematoxylin	Sakura Finetek Japan	Cat# 9130-4P
1% Eosin Y Solution	FUJIFILM Wako	Cat# 051-06515
<b>Critical commercial assays</b>		
QIAamp viral RNA mini kit	Qiagen	Cat# 52904
Luciferase Assay System	Promega	Cat# E8130
SuperScript™ III First-Strand Synthesis System for RT-PCR	Invitrogen	Cat# 11904018
ONE-Glo™ EX Luciferase Assay System	Promega	Cat# E8110
DNA Ligation Kit Ver.2.1	TaKaRa Bio	Cat# 6022
<b>Deposited data</b>		
Viral genome sequence of B-1 strain	This paper	NCBI: LC603286
Viral genome sequence of A50-18 strain	This paper	NCBI: LC603287
Viral genome sequence of H50-11 strain	This paper	NCBI: LC603288
Viral genome sequence of L50-33 strain	This paper	NCBI: LC603289

Viral genome sequence of L50-40 strain	This paper	NCBI: LC603290
Experimental models: Cell lines		
Human: 293T cells	ATCC	Cat# CRL-3216; PRID: CVCL_0063
Green monkey: Vero cells	ATCC	Cat# CCL-81; RRID: CVCL_0059
Green monkey: Vero cells with constitutive expression of TMPRSS II, VeroE6-TMPRSS II cells	Japanese Collection of Research Bioresources Cell Bank	Cat# JCRB1819; RRID: CVCL_YQ49
Syrian hamster: BHK-21(C-13) cells	Japanese Collection of Research Bioresources Cell Bank	Cat# JCRB9020; RRID: CVCL_1915
Syrian hamster: BHK-21(C-13) cells with constitutive expression of hACE2, BHK-hACE2 cells	This paper	N/A
Experimental models: Organisms/strains		
Syrian hamster (male, 5 weeks old)	SLC	Slc:Syrian
Oligonucleotides		
CoV-2-F1-Fw (CTATATAAGCAGAGCTCGTTTAGTGAACCGTattaaggtttatacctcccaggaac)	Torii, et al. (2021)	N/A
CoV-2-F1-Rv (cagattcaactgcatggcattgtagtagcctatttaaggctcctgc)	Torii, et al. (2021)	N/A
CoV-2-F2-Fw (gcaggagcctaaataaggctactaacaatgccatgcaagttgaatctg)	Torii, et al. (2021)	N/A
CoV-2-F2-Rv (ggtaggatttccactacttctcagagactggttttagatcttcgaggc)	Torii, et al. (2021)	N/A
CoV-2-F3-Fw (gcctgccaagatctaaaccagtctctgaagaagtagtgaaaaatcctacc)	Torii, et al. (2021)	N/A
CoV-2-F3-Rv (gggtcacagcgcagcttctcaaaagtactaaagg)	Torii, et al. (2021)	N/A
CoV-2-F4-Fw (caccactaattcaacctattggctgttgacatatcagcatctatagtagctggg)	Torii, et al. (2021)	N/A
CoV-2-F4-Rv (gtttaaaaacgattgtgcatcagctgactg)	Torii, et al. (2021)	N/A

CoV-2-F5-Fw (cacagtctgtaccgtctgcggtatgtggaagggtatggctgtagttgtgat c)	Torii, et al. (2021)	N/A
CoV-2-F5-Rv (gcggtgtgtacatagcctcataaaactcaggtccaataccttgaagtg)	Torii, et al. (2021)	N/A
CoV-2-F6-Fw (cactcaaggtattgggaacctgagttttatgaggctatgtacacaccgc)	Torii, et al. (2021)	N/A
CoV-2-F6-Rv (catacaaaactgccaccatcacaccaggcaagtaaggttagatagca ctctag)	Torii, et al. (2021)	N/A
CoV-2-F7-Fw (ctagagtctatctaaccttaactgcctggttggatggggcagttgtatg )	Torii, et al. (2021)	N/A
CoV-2-F7-Rv (ctagagactagtggaataaaacaagaaaaacaacattgttcgtttagt tgtaac)	Torii, et al. (2021)	N/A
CoV-2-F8-Fw (gtaacaactaaacgaacaatgttgttttctgttttattgccactagtctcta g)	Torii, et al. (2021)	N/A
CoV-2-F8-Rv (gcagcaggatccacaagaacaacagcccttgagacaactacagcaa ctgg)	Torii, et al. (2021)	N/A
CoV-2-F9-Fw (ccagttgctgtagttgtctcaagggtgtgtctgtggatcctgctgc)	Torii, et al. (2021)	N/A
CoV-2-F9-Rv (caatctccattggtgctctcatc)	Torii, et al. (2021)	N/A
CoV-2-F10-Fw (gatgaagagcaaccaatggagattg)	Torii, et al. (2021)	N/A
CoV-2-F10-Rv (GGAGATGCCATGCCGACC Cttttttttttttttttttttgtcattctcctaag)	Torii, et al. (2021)	N/A
CoV-2-Linker-Fw (cttaggagaatgacaaaaaaaaaaaa aaaaaaaaaaaaGGGTCCGCATGGCATCTCC)	Torii, et al. (2021)	N/A
CoV-2-Linker-Rv (gttacctggaaggtataaacctttaatA CGGTTCACTAAACGAGCTCTGCTTATATAG)	Torii, et al. (2021)	N/A
CoV-2-TS-F6-Rv (catacaaaactgccaccatcacaccaggcaagtaaggttagatagcac tctag)	This paper	N/A

CoV-2-TS-F7-Fw (ctagagtgcctatctaaccttaactgcctgggttgatagggcagttgtatg )	This paper	N/A
CoV-2-4052T-Fw (tatattgacattaatggcaatttccatccagattctgcca)	This paper	N/A
CoV-2-4052T-Rv (ttgccattaatgtcaatataaagtaacaagtttctgtga)	This paper	N/A
CoV-2-18782T-Fw (tgattgatgtcaacaatgggttttacaggaacctaca)	This paper	N/A
CoV-2-18782T-Rv (ccattgttgaacatcaatcataaacggattatagacgtaa)	This paper	N/A
CoV-2-19285A-Fw (aaccttaactgcctgggttgatagggcagttgtatg)	This paper	N/A
CoV-2-19285A-Rv (caaccaggcaagtaaggttagatagcactctagtgtcaa)	This paper	N/A
CoV-2-19550T-Fw (tctcgatgctataacatgatgatctcagttggcttagc)	This paper	N/A
CoV-2-19550T-Rv (tcatgttataagcatcgagatacaatctgtactcattagc)	This paper	N/A
CoV-2-20857A-Fw (ctgtaccctataatgagaattatacatttgggtgctggttct)	This paper	N/A
CoV-2-20857A-Rv (tctcatattataggtacagctaatgtaatgtgtttaa)	This paper	N/A
CoV-2-G2-Fw (cggcagtgaggacaatcagacaactac)	Torii, et al. (2021)	N/A
CoV-2-G2-Rv (ggcttagcataattagctatagatcccaaggac)	Torii, et al. (2021)	N/A
CoV-2-G6-Fw (tgtagatgatatcgtaaaaaagatgggtacac)	Torii, et al. (2021)	N/A
CoV-2-G6-Rv (aacgtgtatacacgtagcagactttagtggtac)	Torii, et al. (2021)	N/A
CoV-2-G7-Fw (aaaggtcaacacatggtgttaaagctgc)	Torii, et al. (2021)	N/A
CoV-2-G7-Rv (cgtacacttgttctgagagagggtc)	Torii, et al. (2021)	N/A
covid-dp-4655-4683r (ggcactttgagagatctcatataccgagc)	Torii, et al. (2021)	N/A
covid-dp-18160-18186f (gttgacatacctggcatacctaaggac)	Torii, et al. (2021)	N/A
covid-dp-19712-19738r (caacaccatcaactttgtgtaaacag)	Torii, et al. (2021)	N/A
covid-dp-20470-20496f (gcgcaaacagggtcatctaagtgtgtg)	Torii, et al. (2021)	N/A
Recombinant DNA		

PB-CMV-MCS-EF1-RedPuro	Systembiosciences	Cat# PB514B-2
pCSII-sars-cov-2 F1+2	This paper	N/A
pCSII-sars-cov-2 F3	This paper	N/A
pCSII-sars-cov-2 F4	This paper	N/A
pCSII-sars-cov-2 F5	This paper	N/A
pcDNA3.1.-sars-cov2 F6	This paper	N/A
pcDNA3.1.-sars-cov2 F7	This paper	N/A
pCSII-sars-cov-2 F8	This paper	N/A
pCSII-sars-cov-2 F9	This paper	N/A
pCSII-sars-cov-2 F10+11+12	This paper	N/A
Software and algorithms		
PRISM	GraphPad Software	Version 7.02
Pymol	Schrodinger	<a href="https://www.pymol.org/">https://www.pymol.org/</a>
AlphaFold2	Jumper, et al. (2021)	N/A